1988

Spectral densities and nuclear spin relaxation in solids

Peter A. Beckmann
Bryn Mawr College, pbeckman@brynmawr.edu

Citation

Beckmann, Peter A. 1988. "Spectral densities and nuclear spin relaxation in solids." Physics Reports 171. 3: 85-128.

SPECTRAL DENSITIES AND NUCLEAR SPIN RELAXATION IN SOLIDS

Peter A. BECKMANN

Department of Physics, Bryn Mawr College, Bryn Mawr, Pennsylvania 19010, USA

NORTH-HOLLAND – AMSTERDAM

PHYSICS REPORTS (Review Section of Physics Letters) 171, No. 3 (1988) 85–128. North-Holland, Amsterdam

SPECTRAL DENSITIES AND NUCLEAR SPIN RELAXATION IN SOLIDS

Peter A. BECKMANN

Department of Physics, Bryn Mawr College, Bryn Mawr, Pennsylvania 19010, USA

Received July 1988

Contents:

Abstract:

We investigate the properties of ten spectral densities relevant for nuclear spin relaxation studies in solids. This is preceded by a brief review of nuclear spin relaxation in solids which includes a discussion of the appropriate spin-dependent interactions and the various relaxation rates which can be measured. Also, the link between nuclear spin relaxation and dielectric relaxation is discussed. Where possible and/or appropriate each of the spectral densities is expressed as a continuous distribution of Bloembergen–Purcell–Pound (or Debye) spectral densities $2\xi/(1+\xi^2\omega^2)$ for nuclear Larmor angular frequency ω and correlation time ξ. The spectral densities are named after their originators or the shape of the distributions of correlation times or both and are (1) Bloembergen–Purcell–Pound or δ-function, (2) Havriliak–Negami, (3) Cole–Cole, (4) Davidson–Cole, (5) Fang, (6) Fuoss–Kirkwood, (7) Bryn Mawr, (8) Wagner or log-Gaussian, (9) log-Lorentzian, and (10) Fröhlich or energy box. The Havriliak–Negami spectral density is related to the Dissado–Hill theory for dielectric relaxation. The spectral densities are expressed in a way which makes them easy to compare with each other and with experimental data. Many plots of the distributions of correlation times and of the spectral densities vs. various correlation times characterizing the distributions are given.

Single orders for this issue

PHYSICS REPORTS (Review Section of Physics Letters) 171, No. 3 (1988) 85–128.

Copies of this issue may be obtained at the price given below. All orders should be sent directly to the Publisher. Orders must be accompanied by check.

Single issue price Dfl. 33.00, postage included.

1. Introduction

Nuclear spin relaxation (NSR) experiments in condensed matter provide information concerning dynamical processes. The technique is direct and inevasive because the "tagged" nuclei are usually naturally occurring (e.g., ^{1}H, ^{19}F) or can be substituted (e.g., ^{2}H, ^{13}C) for naturally occurring ones without changing the dynamical processes in an appreciable manner. In general, one can study translational and rotational motions in a variety of condensed phases. For condensed phases whose "lattice points" are extended molecules, the internal motions of subgroups can be studied. The frequency domain available to the experimentalist is very large, running from very slow motions ($\sim$10 Hz) to relatively fast motions ($\sim 10^{12}$ Hz or less) depending on the type of relaxation rate measured. These matters have been extensively dealt with in a series of texts and review articles [1–21]. Dynamical information is also available from nuclear magnetic resonance lineshape studies [1, 7, 11–13, 22–26]. We do not discuss this latter topic in this review.

In liquids, NSR experiments can be very difficult to interpret because the effects of translational, rotational and intramolecular motions are usually very difficult to separate [27, 28]. In oriented liquids, the situation is also very complicated although simple models can be formulated and tested [29, 30]. Even in the solid state, if whole molecule and intramolecular motions are superimposed, they can be very difficult to separate [31]. The situation in polymers is particularly complicated [7, 32, 33]. In many solids, however, the experimentalist generally has a greater degree of selectivity as far as which molecular and intramolecular motions can be studied because systems, temperature ranges and other experimental parameters can be chosen to permit observation of specific motions. Also, there are several different kinds of NSR rates which can be measured, each one probing a different timescale [34]. In the simplest case of a single, one-dimensional motion, like the reorientation of a subgroup about an axis fixed to a molecule which, in turn, is immobile on the frequency scale selected, detailed realistic theoretical models can be formulated and NSR experiments can test these models. For methyl reorientation, for example, one can sort out the difference between quantum mechanical hopping processes at lower temperatures and thermally activated reorientation at higher temperatures [35, 36], one can investigate the consequences of nuclear spin symmetry [35], one can investigate the nature of correlation functions for molecular reorientation [37] and one can investigate details of the local electrostatic potentials [38]. Finally, NSR processes can be used to investigate the role of symmetry in spin–heat-bath interactions and the relationship between the symmetry and Berry's phase [39].

In general, a NSR rate R can be expressed as a sum of spectral densities $\mathcal{J}$ [9, 21]: $R = \Sigma_i \mathcal{J}_i(\omega_i)$ with the $\mathcal{J}_i$ evaluated at specific frequencies ω_i. We review this briefly below. These spectral densities $\mathcal{J}_i$ are the Fourier transforms of the time correlation functions $\mathcal{G}_i(t)$ [9, 19, 21]. The number of terms in the above sum and the frequencies ω_i depend on the details of the motion, the interactions that are being modulated and the specific relaxation rate being measured. Determining the form of the spectral density is an important problem. It depends on the details of the dynamical process and the fact that the observations are being made on an ensemble of potentially interacting molecules or molecular subunits. This is a many-body problem. Determining the form of the spectral density from a relaxation experiment is the dynamical equivalent of determining a line shape from a spectroscopy experiment.

Before presenting and discussing the spectral densities used in solid state NSR in considerable detail in section 6, we review the relevant nuclear spin interactions in section 2, the observable spin–lattice relaxation rates in section 3, the link between NSR and dielectric relaxation in section 4 and the reason why simple motional models are not adequate in solids (even though the fundamental processes may be random) in section 5. The matters discussed in sections 1–5 have been well attended to elsewhere and

the only purpose of our brief review of these topics is to link the physical interactions involved with the spectral density problem in solid state NSR.

2. Nuclear spin interactions in solids

2.1. Introduction

Very general approaches are given in the classic texts of Abragam [21] and Slichter [9]. The Hamiltonian for a nuclear spin system can be written

$$\mathcal{H} = \mathcal{H}_0 + \mathcal{H}_{\text{local}}(t)\,, \tag{1}$$

where the Zeeman term,

$$\mathcal{H}_0 = -\boldsymbol{p}\cdot\boldsymbol{B}_0 = -\gamma\hbar\boldsymbol{I}\cdot\boldsymbol{B}_0 = -\gamma\hbar B_0 I_z\,, \tag{2}$$

characterizes the interaction of the spins of magnetic moment $\boldsymbol{p} = \gamma\hbar\boldsymbol{I}$ and nuclear spin operator $\boldsymbol{I}$ with an applied time-independent magnetic field of magnetic field strength [40, p. 36] $\boldsymbol{B}_0 = B_0\hat{z}$. γ is the magnetogyric ratio of the nucleus. There is no time dependence in this Hamiltonian. Its eigenvalues are the Zeeman levels,

$$E_m = -m\gamma\hbar B_0 = -m\hbar\omega_{\text{L}} \tag{3}$$

which defines the Larmor angular frequency, ω_{L}. In a classical picture, the spins precess about $\boldsymbol{B}_0$ at the frequency $\omega_{\text{L}}/(2\pi)$.

In eq. (1), $\mathcal{H}_{\text{local}}(t)$ represents the local spin-independent interactions. It is broken into time-dependent and time-independent terms via

$$\begin{aligned}\mathcal{H}_{\text{local}}(t) &= \langle\mathcal{H}_{\text{local}}(t)\rangle_t + (\mathcal{H}_{\text{local}}(t) - \langle\mathcal{H}_{\text{local}}(t)\rangle_t)\\ &= \mathcal{H}_{\ell 0} + \mathcal{H}_{\ell}(t)\,.\end{aligned} \tag{4}$$

The time-independent Hamiltonian $\mathcal{H}_{\ell 0}$ has eigenvalues which are usually small compared with those of the Zeeman term and its major effect in solids is to broaden the resonance line (spectrum). (The quadrupolar interaction can be stronger than the Zeeman interaction, even at fairly high fields [3] and the dipolar interaction can be stronger than the Zeeman interaction at low or zero field [41, 42] but we do not include these cases in this general discussion.) The term $\mathcal{H}_{\ell}(t)$ in eq. (4) causes transitions between the spin states. If a spin system has been perturbed, $\mathcal{H}_{\ell}(t)$ will result in relaxation to an equilibrium distribution of populations, the latter being determined by the temperature of the lattice or heat bath. It follows from eq. (3) that transitions involving $|\Delta m| = 1$ yield the quantum condition $\Delta E = \hbar\omega_{\text{L}}$.

We briefly review the four major spin-dependent electromagnetic interactions which can cause relaxation in solids: spin–rotation, chemical shielding, dipolar, and quadrupolar. More detailed forms for the Hamiltonians, relevant for NSR experiments, are given elsewhere [1, 3, 5, 10–12]. We give a brief physical basis for the interaction and we present the Hamiltonian in a form which allows us to link

it to the spectral density. The interactions are divided into two types, those which are linear in the nuclear spin operators (rank one) and those which are quadratic in the nuclear spin operators (rank two).

2.2. Rank-one spin interactions

2.2.1. The spin–rotation interaction

The fundamental physical basis of the spin–rotation interaction is discussed in detail by Ramsey [43]. The electrons in the atoms of a molecule or an intramolecular subunit give rise to a molecular magnetic moment and the molecular rotation makes this magnetic moment time dependent. This rotating moment produces a magnetic field $\boldsymbol{B}_{sr} = \boldsymbol{C} \cdot \mathcal{J}$ at the site of the nucleus where $\boldsymbol{C}$ is the spin–rotation tensor and $\mathcal{J}$ is the molecular angular momentum operator. The Hamiltonian is

$$\mathcal{H}_{sr} = -\gamma\hbar \boldsymbol{I} \cdot \boldsymbol{C} \cdot \mathcal{J} . \tag{5}$$

If the molecule or molecular subunit reorients due to some dynamical process, $\boldsymbol{B}_{sr}$ is time-dependent, the interaction is modulated and NSR can occur. In solids, the spin-rotation interaction can be important for spin-$\frac{1}{2}$ nuclei like ^{13}C but, because of the small moment of inertia, not for ^{1}H.

2.2.2. The chemical shielding interaction (chemical shift anisotropy interaction)

The fundamental physical basis of the chemical shielding interaction is also discussed in detail by Ramsey [43]. Others [3, 5, 9] give a detailed account more relevant to NSR studies. The applied field $\boldsymbol{B}_0$ induces atomic currents which gives rise to a magnetic field $\boldsymbol{B}_{cs} = -\boldsymbol{\sigma} \cdot \boldsymbol{B}_0$ at the site of the nucleus. The Hamiltonian is

$$\mathcal{H}_{cs} = \gamma\hbar \boldsymbol{I} \cdot \boldsymbol{\sigma} \cdot \mathcal{J} . \tag{6}$$

The magnitude and direction of the field $\boldsymbol{B}_{cs}$ depends on the relative orientation of the principal axis of the chemical shift tensor $\boldsymbol{\sigma}$ and the applied magnetic field $\boldsymbol{B}_0$. In a solid, $\boldsymbol{\sigma}$ can be highly anisotropic because of the time-independent anisotropic distribution of electrons (i.e., bonding). Molecular motion makes $\boldsymbol{\sigma}$ time-dependent and the interaction is modulated. Both the chemical shielding and spin–rotation interactions involve atomic currents and can be related [43]. The chemical shielding interaction is important for spin-$\frac{1}{2}$ nuclei like ^{31}P where the magnetic shielding of electrons is significant and it can play a non-negligible role for ^{13}C in liquids [44]. It usually plays little role in practice for ^{1}H in solids although it can be important in polymers.

2.3. Rank-two spin interactions

2.3.1. The dipolar interaction

The spin–rotation and chemical shielding interactions are complicated because they involve the dynamical details of the electrons and quantum mechanical calculations are technically difficult. The dipolar interaction, on the other hand, involves the interaction between two magnetic dipoles and follows from classical electromagnetic theory [40, 45].

A magnetic dipole $\boldsymbol{p}$ produces a dipolar magnetic field at $\boldsymbol{r}$ given by [40, 45]

$$\boldsymbol{B}_{\mathrm{d}} = -\frac{\boldsymbol{p}}{r^3} + 3\,\frac{(\boldsymbol{p}\cdot\boldsymbol{r})\boldsymbol{r}}{r^5}\,. \tag{7}$$

With magnetic dipole moment $\boldsymbol{p} = \gamma\hbar\boldsymbol{I}$, the Hamiltonian for the interaction between like spins 1 and 2 is

$$\begin{aligned}\mathscr{H}_{\mathrm{d}} &= \boldsymbol{p}_1\cdot\boldsymbol{B}_{\mathrm{d}2} = -\boldsymbol{p}_2\cdot\boldsymbol{B}_{\mathrm{d}1}\\ &= \gamma^2\hbar^2\left(\frac{\boldsymbol{I}_1\cdot\boldsymbol{I}_2}{r^3} - 3\,\frac{(\boldsymbol{I}_1\cdot\boldsymbol{r})(\boldsymbol{I}_2\cdot\boldsymbol{r})}{r^5}\right).\end{aligned} \tag{8}$$

The vector $\boldsymbol{r}$ is the vector from spin 1 to spin 2 (or vice-versa) and it is time dependent as a result of molecular motion. Thus, the interaction is modulated and NSR occurs. The dipolar interaction is usually the dominant NSR mechanism in solids for $I = \frac{1}{2}$ and it is usually the only mechanism of importance for ^{1}H relaxation. In isotropic liquids, this interaction is essentially averaged to zero by the isotropic motion. We discuss the dipolar interaction further after discussing the quadrupolar interaction so both can be cast in the same mathematical form.

2.3.2. The quadrupolar interaction

The fundamental physics of the quadrupolar interaction is discussed by Ramsey [43]. Abragam [21] and Slichter [9] discuss it in relation to NSR. There is an interaction between the electric quadrupole moment of the nucleus and an electric field gradient $\nabla\mathscr{E}$ at the site of the nucleus. Only nuclei with $I > \frac{1}{2}$, like ^{2}H and ^{14}N (both with $I = 1$), possess a non-zero electric quadrupole moment so the interaction plays no role for spin-$\frac{1}{2}$ nuclei such as ^{1}H, ^{19}F and ^{13}C. Although it is basically an electric interaction, it depends on the quantum state of the nucleus but the electric states and the magnetic (spin) states of the nucleus are symmetry related. Since the nuclear spin state projection quantum number m_I is specified with respect to the applied magnetic field $\boldsymbol{B}_0$, the interaction depends on the relative orientation of $\boldsymbol{B}_0$ and $\nabla\mathscr{E}$. $\nabla\mathscr{E}$ arises from the local electron distribution and for some cases (e.g., a C–^{2}H bond), $\nabla\mathscr{E}$ will be nearly axially symmetric with the principal axis along the bond direction. If molecular motion modulates $\nabla\mathscr{E}$ by reorienting the bond, the interaction is modulated and the nucleus can change nuclear spin states. In this manner, a perturbed distribution of the nuclear spin states will relax to its equilibrium configuration.

The quadrupolar Hamiltonian takes on many mathematical forms depending on the system of units, the definition of the electric field gradient tensor $\mathscr{V}$, the reference frame chosen and the local symmetry in $\mathscr{V}$. For simplicity, we assume an axial environment (cylindrical symmetry) like that nearly encountered in a C–^{2}H bond. In this case, $\mathscr{V} \equiv \mathscr{V}_{zz} = -\partial\mathscr{E}_z/\partial z$ where $\mathscr{E}_z$ is the component of the electric field along the bond direction. The radial components $\mathscr{V}_{xx} = \mathscr{V}_{yy} = -\partial\mathscr{E}_\rho/\partial\rho$ do not enter into the problem. A more general form for lower symmetry environments can be found in Ramsey [43] and Abragam [21]. In Cartesian form, a generic, if not very useful form for the quadrupolar interaction, given the symmetry discussed above, is

$$\mathscr{H}_{\mathrm{q}} = \frac{(eQ)\mathscr{V}}{4I(2I-1)}\left[3I_z^2 - I(I+1)\right], \tag{9}$$

where eQ is the nuclear electric quadrupole moment. The nuclear spin operator I_z in eq. (9) refers to the *local frame*, the frame in which the electric field gradient is diagonal. It must be transformed into the applied magnetic field frame before matrix elements can be calculated and the angles involved in this transformation will be time-dependent as the relevant bond in a molecule or molecular sub-unit moves. Thus, the interaction is modulated and NSR can occur.

2.3.3. The dipolar and quadrupolar interactions in spherical tensor form

To calculate NSR, it is convenient to put the spin-dependent interactions into spherical tensor form. In this way, it is straightforward to change from molecular to laboratory frames. It also allows for a separation of spatial and spin variables in most cases of practical interest and this, in turn, allows for a clear distinction between the time-independent spin matrix elements and the time-dependent spatial matrix elements. The time dependence of the spatial matrix elements can be treated classically via correlation functions without effecting the precise quantum mechanical treatment of the spin system [46]. This has the consequence that the strength of NSR rates can often be calculated quite accurately which leaves motional parameters as the only unknowns to be determined from experiments.

The dipolar and quadrupolar interactions are bilinear in the nuclear spin operators and have the same form and symmetry when cast in spherical tensor form. The Hamiltonian is

$$\mathcal{H} = \sum_{\mu=-2}^{+2} (-1)^{\mu} F_{2,\mu} T_{2,-\mu} , \tag{10}$$

where F_2 is a spherical tensor of rank two [47, 48] specifying the spatial part of the interaction. T_2 is a spherical tensor of rank two and can be formed from the contraction of the spherical vector operators $I^{(1)}$ and $I^{(2)}$ [47];

$$T_{2,\mu} = \sum_{\nu=-1}^{+1} C(1,1,2;\, \nu,\, \mu-\nu) I^{(1)}_{1,\nu} I^{(2)}_{1,\mu-\nu} , \tag{11}$$

where $C(I_1, I_2, I; m_1, M - m_1)$ is a Clebsch–Gordan coefficient [47]. The components of the spherical tensor operators of rank one (spherical vector operators) are related to components of the Cartesian vector operators by [47],

$$I_0 = I_z \quad \text{and} \quad I_{\pm 1} = \mp(\tfrac{1}{2})^{1/2}(I_x \pm \mathrm{i} I_y) . \tag{12}$$

For the dipolar interaction between like spins, $I^{(1)}$ and $I^{(2)}$ refer to different but identical spins and eq. (11) can be interpreted physically in terms of the addition of the components of two angular momentum vectors. For the quadrupolar interaction, eq. (11) may be useful for mathematical convenience but $I^{(1)}$ and $I^{(2)}$ refer to the same nucleus and the fundamental nuclear property is the second rank tensor T_2. Either way, the labels (1) and (2) can be dropped. The labels must be kept for the dipolar interaction between unlike spins because in this case there are different Larmor frequencies involved and the relaxation equations are slightly different [21]. We do not treat this case in this brief introductory review but the extension to this case is straightforward and the main discussion concerning the spectral densities in section 6 is the same.

The chemical shielding and spin–rotation interactions can also be cast in the form of eq. (10) but they are linear in the nuclear spin operators so $T_{2,\mu}$ becomes $T_{1,\mu}$ which is just $I_{1,\mu}$, $F_{2,\mu}$ is replaced by

$F_{1,\mu}$ and $\mu = -1, 0$ and $+1$. The spherical tensor form of these interactions can be found elsewhere [11, 12, 49].

For the dipolar interaction, we assume that the distance r is independent of time. Thus, the vector $\boldsymbol{r}(t) = \boldsymbol{r}(r, \theta(t), \phi(t))$ and the only time dependence is in the angles $\Omega = \theta, \phi$ which specify the spin–spin vectors relative to the applied magnetic field $\boldsymbol{B}_0$. This is the case in those areas of solid state NSR research where useful information is being learned about the spectral density because otherwise the distance $r(t)$ appears in the spectral density and not in a time-independent constant. Two examples are the ^{1}H–^{1}H interaction in a methyl group (an equilateral triangle of protons) and the ^{13}C–^{1}H interaction in a CH bond. (Again, in this introductory section of this review, we are not considering the latter case which involves the dipolar interaction between unlike spins.) For the quadrupolar interaction, we assume that $\mathscr{V}$ is constant. In practice, this is a good approximation for a large class of systems.

With these simplifying assumptions, F_2 for the dipolar and quadrupolar interactions is given by

$$F_{2,\mu}(\theta, \phi) = -(6)^{1/2}\mathscr{B}(4\pi/5)^{1/2}Y_{2,\mu}(\theta, \phi)\,, \tag{13}$$

where $\mathscr{B}$ is

$$\mathscr{B} = \gamma^2\hbar^2/r^3 \tag{14}$$

for the dipolar interaction and

$$\mathscr{B} = \tfrac{1}{4}(eQ)\mathscr{V} \tag{15}$$

for the quadrupolar interaction.

In eq. (13), Y_2 is a second order spherical harmonic [47]. Equation (13) can also be expressed in terms of Wigner Rotation Matrices of rank two, D^2, whose normalization is sometimes preferable [47]. In this case, the right-hand side of eq. (13) is $-(6)^{1/2}\mathscr{B}D^{2*}_{\mu 0}(\phi, \theta, 0)$ using Rose's definition for the D matrices [47]. The spherical angles $\theta(t)$, $\phi(t)$ specify the orientation of $\boldsymbol{r}$ with respect to $\boldsymbol{B}_0$ for the dipolar interaction and they specify $\boldsymbol{\nabla\mathscr{E}}$ with respect to $\boldsymbol{B}_0$ for the quadrupolar interaction.

3. Nuclear spin relaxation

3.1. General theory

3.1.1. The correlation function

A detailed account of the theory of NSR can be found in Abragam [21] and Slichter [9]. Our purpose here is to relate the Hamiltonian for the relevant interaction to the NSR rate via the spectral density. We assume the interaction has been cast into spherical tensor form as in eq. (10). We have done this for the rank-two interactions and it is done for the rank-one interactions elsewhere [11, 12, 49].

NSR is caused by the time dependence in the spatial part of the spin-dependent interaction. Thus, the tensor $F_{2,\mu}\{\Omega(t)\}$ with $\Omega(t) = \theta(t)$, $\phi(t)$ in eq. (10) is time dependent and the interaction is modulated. The Hamiltonian in eq. (10) is treated as a perturbation. To see the connection between the

Hamiltonian and the relaxation rate, we define an autocorrelation function $\mathcal{G}(t)$ by [21]

$$\mathcal{G}_{\ell,\mu}(t) = \int_{\Omega_1}\int_{\Omega_2} \mathcal{P}(\Omega_1)P(\Omega_1, \Omega_2, t)[F_{\ell,\mu}(\Omega_1)F^*_{\ell,\mu}(\Omega_2)]\,\mathrm{d}\Omega_1\,\mathrm{d}\Omega_2\,. \tag{16}$$

For the dipolar and quadrupolar interactions, $\ell = 2$ and for the chemical shielding and spin–rotation interactions, $\ell = 1$. $\mathcal{P}(\Omega_1)$ is the probability that the angles Ω take on the values Ω_1 at $t = 0$ and $P(\Omega_1, \Omega_2)$ is the conditional probability that $\Omega = \Omega_2$ at time t if $\Omega = \Omega_1$ at $t = 0$. For the chemical shielding and spin–rotation interactions, Ω is replaced by appropriate components of $\boldsymbol{\sigma}$ and $\boldsymbol{C}$, respectively, but with appropriate symmetry based simplifications, these variables can again be written in terms of angles whose time dependence characterizes the motion.

Confining ourselves to the rank two interactions, we define the reduced correlation function $G_\mu(t)$ by

$$\mathcal{G}_{\ell,\mu}(t) = (24\pi/5)\mathcal{B}^2 G_\mu(t)\,, \tag{17}$$

from which it follows that

$$G_\mu(t) = \int_{\Omega_1}\int_{\Omega_2} \mathcal{P}(\Omega_1)P(\Omega_1, \Omega_2, t)[Y_{2,\mu}(\Omega_1)Y^*_{2,\mu}(\Omega_2)]\,\mathrm{d}\Omega_1\,\mathrm{d}\Omega_2\,. \tag{18}$$

Since $\ell = 2$, we suppress ℓ in $G_{\ell,\mu}$. In essence, eq. (18) contains the conveniently normalized time-dependent parts of the spatial matrix elements of the Hamiltonian in eq. (10).

If the motion is random and *if* one is dealing with an ensemble of equivalent dynamical units, *then* $\mathcal{P}(\Omega_1) = 1/(4\pi)$ and $P(\Omega_1, \Omega_2, t)$ is taken as a solution of the diffusion equation. In this case [21],

$$G(t) = \mathrm{e}^{-|t|/\tau}\,, \tag{19}$$

where the correlation time τ is independent of the component μ so we drop the subscripts for convenience. In solids, this form for $G(t)$ is often not successful. The normalization in eq. (17) is chosen to give the normalization in eq. (19).

In general, $G_\mu(t)$ depends on the component μ in two ways. First, as a result of doing first order perturbation theory, there are constant factors coming from the time-dependent parts of the spin and spatial matrix elements. They can be dealt with via other factors discussed below. Second, there are dynamic parameters such as allowing τ to be τ_μ in relationships like eq. (19). In this review, we assume that τ or other parameters describing the motion are independent of μ. This is, in general, a very good approximation in solids, particularly in powders. As mentioned below, this is not a good approximation for certain kinds of correlated motions in oriented liquids.

3.1.2. The spectral density

A nuclear spin relaxation rate R is of the form

$$R(\{\omega_j\}, \{x_i\}) = \mathcal{A}q(\{\omega_j\}, \{x_i\})\,. \tag{20}$$

A simple physical interpretation of eq. (20) is obtained from Fermi's Golden Rule #2 [50, 51]: R is an appropriately normalized product of the factor $\mathcal{A}$ ($\propto \mathcal{B}^2$ contained in eq. (17) and given by eqs. (14) or

(15)) which is the square of the time-independent parts of the matrix elements (spin as well as space) and a factor q which is a linear combination of spectral densities, or, equivalently, densities of states or the power spectra of the local magnetic fields.

For the dipolar interaction, the factor $\mathscr{A}$ is chosen to be

$$\mathscr{A} = \frac{1}{5}\,\frac{1}{\hbar^2}\,I(I+1)\left(\frac{\gamma^2\hbar^2}{r^3}\right)^2 . \tag{21}$$

The factor $\mathscr{B}^2$ (with $\mathscr{B}$ given by eq. (14)) enters and the factor $I(I+1)$ comes from the (square of) nuclear spin matrix elements that appear in the perturbation calculation. It should be mentioned that NSR due to dipolar interactions is not always an exponential process in which case R is not uniquely defined via eq. (20). A dipolar coupled spin system can lead to the case where the NSR process is a sum of exponentials but this is unusual. More common is that correlated motions can lead to nonexponential relaxation. The best example here is a fixed triangle of spin-$\frac{1}{2}$ protons (a methyl group) [52–54]. We do not deal with the general case of non-exponential relaxation in this review but often a physically meaningful relaxation rate can be determined from the initial decay in the relaxation process [52]. In this case, this class of phenomena can be included in the present discussion.

In general, NSR due to quadrupolar interactions is not an exponential process for $I>1$ [21, 55, 56] and the simplifying assumptions we have been making break down. However, for the very important case of $I=1$, this procedure is valid, the relaxation is exponential, and the parameter $\mathscr{A}$ is given by

$$\mathscr{A} = \frac{3}{80}\left(\frac{eQ\mathscr{V}}{\hbar}\right)^2 . \tag{22}$$

Again, the factor $\mathscr{B}^2$ in eq. (15) enters and since $I=1$, there are no other physical constants.

The function q in eq. (20) can be written

$$q(\{\omega_j\},\{x_i\}) = \sum_j n_j J(\omega_j,\{x_i\}) . \tag{23}$$

The set of frequencies $\{\omega_j;\ j=1,2,3,\ldots\}$ usually contains the nuclear Larmor frequency $\omega_1 \equiv \omega_L = \gamma B_0$ but other frequencies may be relevant as discussed below in a few examples. The parameter set $\{x_i;\ i=1,2,3,\ldots\}$, characterizes the dynamical process or processes involved and much will be said of such matters later. In the simple example given in eq. (19), $x_1=\tau$ is the only parameter. The factors n_j in eq. (23) are appropriately normalized ratios of squares of time-independent parts of matrix elements and some examples are given below. They are chosen to renormalize G_μ such that it is independent of the component μ. Their values are partially determined by the definition of $\mathscr{A}$.

The spectral density $J(\omega,\{x_i\})$ may depend on many molecular variables $\{x_i\}$ but each J depends on only one frequency. (For the dipolar interaction between unlike spins, this single frequency may be a sum or difference frequency.) $J(\omega)$ is the Fourier transform of the correlation function $G(t)$ in eq. (18);

$$J(\omega,\{x_i\}) = \int_{-\infty}^{\infty} G(t,\{x_i\})\,e^{i\omega t}\,dt . \tag{24}$$

With the normalization adopted for $G(t)$,

$$\int_0^\infty J(\omega)\,\mathrm{d}\omega = \pi\,. \tag{25}$$

For the random motion case with G given by eq. (19), the spectral density is

$$J_{\mathrm{BPP}}(\omega, \tau) = 2\tau/(1+\omega^2\tau^2)\,. \tag{26}$$

As stated above, only the single parameter $x_1 = \tau$, the correlation time, is required to characterize the motion. This approach was first used in relaxation NMR by Bloembergen, Purcell and Pound (BPP) in their classic paper [57] which, with the classic paper of Bloch [58], started this field. The work of Kubo and Tomita [59] put this spectral density on a more solid theoretical foundation.

3.2. Relaxation rates for the dipolar and quadrupolar interactions

As an example of specific forms for the relaxation rate expressed in eqs. (20)–(23), we investigate the dipolar interaction for like spins where r is time-independent as discussed previously and the quadrupolar interaction for $I = 1$ where the electric field gradient is axially symmetric and constant in its local frame. The dipolar interaction is usually only relevant for spin-$\frac{1}{2}$ since the quadrupolar interaction usually dominates for spin $>\frac{1}{2}$. The four relaxation rates discussed here are all spin–lattice relaxation rates and involve the interaction between the nuclear spin system and the thermal heat bath which is assumed to have infinite heat capacity. This is always true in practice given the extremely small magnitude of nuclear spin energies.

3.2.1. Zeeman relaxation

The degree of Zeeman order is determined by the difference in populations between adjacent Zeeman levels. At equilibrium, this difference is characterized by the temperature of the heat bath (lattice) via the Boltzmann factor. The temperature of the bath is one of the non-spin parameters contained directly or indirectly in the parameter set $\{x_i\}$. This is discussed further below. The Zeeman relaxation rate characterizes the rate at which a perturbed spin system comes to equilibrium with the environment. Since the dipolar and quadrupolar interactions are bilinear in the spin operators, both single and double quantum transitions occur. (For the dipolar interaction, a double quantum transition means two single quantum transitions.) R_Z is given by

$$R_Z = \mathscr{A}[J(\omega_L) + 4J(2\omega_L)]\,, \tag{27}$$

which means that in eq. (23), $n_1 = 1$, $n_2 = 4$, $\omega_1 = \omega_L$ and $\omega_2 = 2\omega_L$. For an ensemble of dipolar coupled spin pairs where each pair is isolated from all other pairs but is in contact with the heat bath, the factor $\mathscr{A}$ is given by eq. (21). More generally, $\mathscr{A}$ is of this order of magnitude for a range of nuclear spin geometries. (See, for example, R_Z for the three protons in a methyl group [60] or for the nine protons in a *t*-butyl group [37, 61, 62].) For the quadrupolar interaction, eq. (22) is always valid (given the symmetries and assumptions discussed earlier) since $\mathscr{H}_q$ is a local interaction only.

3.2.2. Dipolar order relaxation

If the spins are strongly interacting then the time-independent part of the dipolar interaction (see eq. (4)) is large and there is a significant distribution in static local dipolar fields. In frequency units, this distribution is usually Gaussian with a width in the range of 1–100 kHz for ^{1}H depending on the degree of motion (which reduces the static component). This is to be compared with Zeeman levels which are in the 5–100 MHz range for most ^{1}H NSR experiments (excluding zero-field NMR [41, 42]). Thus the Zeeman levels are broadened into bands with a population distribution given, at equilibrium, by the Boltzmann factor. Experimentally, this distribution can be perturbed and its return to equilibrium monitored as first shown and explained beautifully by Jeener and Broekert [63]. There is no general theory which covers all motional time-scales. The dipolar angular frequency ω_{dip} is defined by $\omega_{dip} = \gamma B_{dip}$ where B_{dip} is an appropriately defined time-independent average local dipolar field. $\omega_{dip}/(2\pi)$ is of the order of a few kHz for ^{1}H. If the motion is characterized by a correlation time τ and is very slow ($\omega_{dip}\tau \gg 1$) then [15, 64]

$$R_{dip} = (2/\tau)(1-p)\,, \tag{28}$$

where $p < 1$ depends on the details of the relaxation process and the factor 2 has its origin in the fact that the dipolar interaction is a pairwise interaction. This case usually arises from diffusional processes [65, 66] and in this case, there is no information about the spectral density. However, for molecular solids where internal reorientation is the dominant motion, $\omega_{dip}\tau \ll 1$ often occurs and

$$R_{dip} = c\mathscr{A}[J(\omega_{dip}) + 2J(\omega_0) + 2J(2\omega_0)]\,. \tag{29}$$

For many cases of practical interest where the spectral density is being measured in the 5–100 MHz range, ω_{dip} may be taken to be zero. The factor multiplying the linear combination of spectral densities depends on the system under study in a not completely understood way since this is a strongly coupled many body problem. This places limitations on the use of R_{dip} experiments. We write this factor $c\mathscr{A}$ where $\mathscr{A}$ is that used in the expression for R_Z in eq. (27) because most theoretical models and experimental results indicate that c is of the order of unity [67–70]. Used in conjunction with Zeeman relaxation rate experiments, R_{dip} can be very helpful, particularly if there are slow motions which will show up in the $J(\omega_{dip})$ term. Slow here means $\omega_0^{-1} \ll \tau \ll \omega_{dip}^{-1}$.

3.2.3. Rotating frame relaxation

Experimentally, a static field can be set up in the frame rotating at the nuclear spin precession (Larmor) frequency ω_0 (the so-called *rotating frame*). The strength of this field is characterized by B_{rot} which defines the angular frequency $\omega_{rot} = \gamma B_{rot}$. The expression for the NSR rate R_{rot} depends on the strength of B_{rot} and the time-scale of the motion. In general, many expressions for R_{rot} have been given and most are for particular geometries or systems [8, 9, 64, 71–76]. If $\omega_{dip}\tau \gg 1$ and $B_{rot} \sim B_{dip}$ then [8, 64, 72]

$$R_{rot} = \frac{2}{\tau}(1-p)\frac{B_{dip}^2}{B_{dip}^2 + B_{rot}^2}\,. \tag{30}$$

Equation (28) for R_{dip} is the special case of R_{rot}, namely when $B_{rot} = 0$. If $B_{rot} \gg B_{dip}$ and $\omega_0^{-1} \ll \tau \ll$

ω_{rot}^{-1} ($\ll\omega_{dip}^{-1}$) then one can measure the relaxation rate [71, 73–76],

$$R_{rot} = \mathscr{A}[\tfrac{3}{2}J(2\omega_{rot}) + \tfrac{5}{2}J(\omega_L) + J(2\omega_L)]\,. \tag{31}$$

R_{rot} experiments are most useful for dipolar coupled systems and $\mathscr{A}$ is again given by eq. (21) with the qualifying remarks discussed in section 3.2.1. The experimenter has control over the frequency ω_{rot} which is in the 2π(50 kHz)–2π(500 kHz) range.

3.2.4. Quadrupolar order relaxation in oriented liquids

We mention this relaxation rate for completeness. Quadrupolar order is produced for $I > \frac{1}{2}$ nuclei in the same way dipolar order is produced for all spin systems, only the effects are much greater. The symmetry must also be non-cubic for quadrupolar relaxation to occur. The spread within each Zeeman level can be in the 1–100 kHz range for ^{2}H [25] and ^{23}Na [26] and in the MHz range for ^{14}N [77, 78]. In normal solids there are no experiments that are able to perturb this order and measure its return to equilibrium. In oriented liquids, however, like liquid crystals, there is a shift [30] as well as a broadening of the Zeeman levels and there is a variety of pulse techniques for perturbing this order and measuring its return to equilibrium [79, 80]. The expression for the observed rate depends on the experiment. This is outside the scope of this review and the reader is referred to other reviews which specifically discuss ^{2}H relaxation in oriented liquids [29, 81].

4. The relationship between dielectric relaxation and nuclear spin relaxation

Many of the spectral densities used in NSR studies have their origin in dielectric relaxation (DR) experiments. In a DR experiment, electric dipoles in a molecule or a molecular subunit are perturbed from an equilibrium configuration by an external electric field produced by a time-dependent voltage applied to a capacitor. In the simplest idealized version of the experiments, the field is removed and the recovery to equilibrium, characterized by the electric susceptibility, is monitored. The rate at which the electric dipoles relax depends on the extent to which the local electric dipole-dependent transitions are modulated by the molecular motion. For the simple case where the motion is described by Poisson statistics, the molecular motion is characterized by a peak loss frequency ω_p which can be varied via the temperature. Very crudely, the experiment is a measure of the mean number of dipoles reorienting at the measuring frequency. A more detailed discussion of DR is given elsewhere [82–86].

NSR experiments monitor nuclear spins rather than electric dipoles and there are many different kinds of experiments. As discussed above, nuclear Zeeman order is determined by an external magnetic field B_0, dipolar order is determined by the distribution of populations within the dipolar broadened Zeeman levels, rotating frame Zeeman order is determined by the populations of the Zeeman levels in the rotating frame created by an applied rotating field, and quadrupolar order is determined by the degree of anisotropy in an oriented liquid. For all these cases, NSR experiments are performed by perturbing the nuclear spin system from the equilibrium distribution among whatever discrete or effectively continuous (dipolar order) levels are appropriate. This is done by an external oscillating magnetic field produced by an oscillating current in an inductor. The field is removed and the recovery to equilibrium is observed via the voltage induced in the same inductor by a changing nuclear magnetization (Faraday's law). There are many tricks of the trade and details of the pulse experiments can be found elsewhere [1, 87]. As discussed previously, the rate at which the nuclear spin system

returns to equilibrium depends on the extent to which the local spin-dependent interactions are modulated by the molecular and intramolecular motion. For the simple case where the motion can be characterized by Poisson statistics, a mean reorientation rate or correlation time τ is the only molecular parameter and it can be varied via the temperature. Very crudely, the experiment is an indirect measure of the average number of mobile units at various frequencies.

There are important differences between NSR and DR. First, different motions might be involved since the two techniques are sensitive to the motions of different vectors. Whereas a DR experiment monitors electric dipole vectors, NSR experiments monitor quite different vectors and/or angles characterizing the spin system as discussed in sections 2.3 and 3.2. This is not a serious problem insofar as using DR spectral densities in NSR work is concerned so long as DR and NSR results in the same material are compared cautiously. Second [7], DR relaxation involves the modulation of rank-one interactions whereas dipole–dipole and quadrupolar NSR involves the modulation of rank-two interactions. Thus the statistics could be fundamentally different. Third [7], there is no analog of spin diffusion in DR. When there are many motions, such as in polymers, the details of the statistical description of the motion may be effected by the degree of spin diffusion [7] but this is not a problem in simple solids with one or a very few identifiable motions. In fact, very strong dipole–dipole couplings in simple systems leads to spin diffusion relaxation rates ($R_2 = T_2^{-1}$) in the $(10\,\mu s)^{-1}$ range which means that all protons, regardless of whether or not they are involved in the motion, relax with the same rate ($R = T_1^{-1}$) which is rarely larger than $(1\,ms)^{-1}$. That is, $T_1 \gg T_2$ and the entire spin system is characterized by a spin temperature throughout the spin–lattice relaxation process.

For the DR case, the complex dielectric susceptibility is

$$\chi(\omega) = \chi'(\omega) - i\chi''(\omega) = \chi'(0)H(\omega)\,, \tag{32}$$

where $H(\omega)$ is the (complex) spectral density. It is essentially a normalized complex dielectric susceptibility. With normalization given by eq. (25), if the DR peak loss frequency ω_p is identified with the inverse of the NSR correlation time τ, then

$$J(\omega) = (2/\omega)\,\mathrm{Im}[H(\omega)]\,, \tag{33}$$

where Im means the imaginary part. The correspondence $\omega_p = \tau^{-1}$ is not necessarily appropriate for any particular motion; we simply make the equality in order to relate the spectral densities used in the two kinds of studies. Thus, if Poisson statistics apply,

$$H(\omega) = [1 + i(\omega/\omega_p)]^{-1} \tag{34}$$

and the NSR spectral density J is given by eq. (26). Equation (34) is referred to as the Debye spectral density [83, 84].

5. Debye and non-Debye nuclear spin relaxation

5.1. Random motion and Debye relaxation

The simplest $J(\omega)$ is that resulting from a single random motion characterized by a single correlation time τ. The NSR rate is given by eq. (26). This J_{BPP} follows in a straightforward way from the assumption that the motion obeys Poisson statistics (i.e., is random) [16, 21].

5.2. Non-Debye relaxation

In solids, eq. (26) is often not realized in practice and it is not always clear how a thermally activated process can result in what is, or what appears to be, a non-Poisson (i.e., non-random) process. There are a variety of spectral densities used to fit experimental data and the main purpose of this paper is to review many of them and to put them into a common format for use in NSR experiments. There are two basic reasons why the *observed* spectral density may not be of the form in eq. (26). First, the motion may be inherently non-random which might be the case if motions are correlated. (This is different from the reason discussed in section 3.1.2 where a single motion (random or not) of a rigid group leads to correlated motions of the vectors whose modulation is responsible for the relaxation.) An example here is the spectral density due to order director fluctuations in oriented liquids where many molecules undergo cooperative motions [88]. Second, within an ensemble of reorienting units (i.e., the whole sample), there may be sub-ensembles, each of which involves units undergoing random motion and each of which is characterized by a BPP spectral density $J_{\mathrm{BPP}}(\omega, \tau)$, but, where each sub-ensemble is characterized by a different correlation time τ. This might be the case in a molecular solid where different internal rotors in the molecule see different electrostatic environments. It also might be the case in an amorphous solid where there is a distribution of environments. The sum of spectral densities each of which is given by eq. (26) is no longer of a form given by eq. (26) in the same way that the resulting correlation function is no longer exponential since a linear combination of exponential correlation functions (eq. (19)) results in a non-exponential correlation function. The need to use a distribution of correlation times or a non-exponential correlation function in NSR experiments has been known for many years [89] and the details of the microscopic physical origins of [90–93], and the statistical mechanics of [94–96] the departure from Debye behaviour have been and are now being studied.

5.3. Distributions of correlation times

From a formal point of view, the case of a distribution of correlation times, each characterizing an exponential correlation function, and the case of a non-exponential correlation function are indistinguishable [97] and one can write

$$J(\omega, x_1, x_2, \ldots) = \int_0^\infty \Lambda(\xi, x_1, x_2, \ldots) \frac{2\xi}{1+\omega^2\xi^2} \, \mathrm{d}\xi \,, \tag{35}$$

where $\Lambda(\xi, x_1, x_2, \ldots)$ is the distribution of correlation times ξ and $\{x_i\}$ is a parameter set which characterizes the distribution of ξ. From a practical point of view, one of the clearest constraints on Λ is that it cannot depend on ω; it is a property of the molecular system under study, not of the measuring apparatus.

Λ is normalized to unity;

$$\int_0^\infty \Lambda(\xi, x_1, x_2, \ldots) \, \mathrm{d}\xi = 1 \,. \tag{36}$$

Since the Fourier transform is a linear operation, Λ also gives the reduced correlation function as a

distribution of exponential correlation functions;

$$g(t, x_1, x_2, \ldots) = \int_0^\infty \Lambda(\xi, x_1, x_2, \ldots)\, \mathrm{e}^{-|t|/\xi}\, \mathrm{d}\xi \,. \tag{37}$$

In the discussion which follows, we shall present several distributions Λ and their associated spectral densities in a consistent and logical manner which is appropriate for the analysis of NSR experiments. Not all the spectral densities have a distribution of correlation times associated with them, however. Some are simply phenomenological in nature. Putting these spectral densities on a more formal footing, or interpreting them as special cases of more general theories, is an important avenue of research.

In all cases where the various $\Lambda(\xi)$ are presented, they satisfy eq. (36) and the resulting spectral densities $J(\omega)$ satisfy eq. (25). Most of the distributions $\Lambda(\xi)$ have a particular correlation time (i.e., $x_1 = \tau$) which characterizes the distribution. This can be a cutoff ξ, or a mean ξ or some similar parametrization of the distribution $\Lambda(\xi)$. In this case the dimensionless parameter $y = \xi/\tau$ is useful as is the distribution $\Delta(y)$ defined by

$$\Delta(y)\, \mathrm{d}y = \Lambda(\xi)\, \mathrm{d}\xi \,, \qquad \Delta(y) = \tau \Lambda[\xi(y)] \,. \tag{38}$$

Although we do not give $\Delta(y)$ for the distributions used in this paper, it is useful as an intermediate mathematical step in the handling of several of the spectral densities.

5.4. Correlation time and activation energy

In practice, the correlation time ξ must be theoretically linked to an experimental observable like temperature T or pressure P and this link is an important area of study. The relationship between ξ and T is usually, though not necessarily, assumed to be an Arrhenius relationship,

$$\xi = \xi_\infty \exp(\zeta/kT) \,. \tag{39}$$

Equation (39) has its origins in the theory of thermally activated processes [98] and whether or not conditions in most solids are consistent with such a simple assumption has been discussed continuously for most of this century [85, 99–108]. The parameter ξ_∞ has been discussed elsewhere [101–106, 108] and it is either temperature independent or only weakly dependent on temperature for most cases of interest (see [104] for an excellent discussion). The parameter ζ is an "apparent" or "effective" activation energy and can often be related to physically relevant activation energies or hindering potentials [103, 105]. Equation (39) is also true for the characteristic $\xi = \tau$ and if $\xi_\infty \equiv \tau_\infty$ is constant for a given motion, then a plot of $\ln J$ vs. $\ln \tau$ has the same general shape as $\ln R$ vs. T^{-1} which is why the latter is the way in which experimental results are usually presented. In this case, the parameter $z = \ln(\xi/\tau) = \ln y$ is useful, as is the distribution function $\theta(z)$ defined by

$$\theta(z)\, \mathrm{d}z = \Lambda(\xi)\, \mathrm{d}\xi \,, \qquad \theta(z) = \tau\, \mathrm{e}^z \Lambda[\xi(z)] \,. \tag{40}$$

It is important to note that with the single exception of the Fröhlich or energy box spectral density discussed in section 6.11, eq. (39) need not be assumed since we deal with correlation times and not

temperature as the independent variable for most of this review. Equation (39) is only presented as the basis for introducing $\theta(z)$ in eq. (40) as a convenient representation of the distribution of correlation times. Of course eq. (39) or some other model-dependent link between the correlation time ξ and an experimental observable (temperature, pressure [109, 110], etc.) must be used to interpret experimental results.

6. The spectral densities

6.1. Introduction

With these introductory remarks and definitions, we proceed with a discussion of ten spectral densities. Some of these spectral densities have been presented before in one form or another, some by Conner [111] and/or Noack and Preissing [112]. The main purpose in the present paper is to add to those given by these authors, to present them in a consistent and convenient way for use in interpreting NSR experiments, to link them theoretically where possible, to discuss their properties in a much more detailed manner than has previously been done and to compare them with each other in detail. Finally, some papers confuse the distribution functions $\Lambda(\xi)$ defined by eqs. (35) and (36) and $\theta(z)$ defined by eq. (40).

A word is in order concerning the format of the plots we present for J vs. τ. (See J vs. τ for J_{BPP} in eq. (26) in fig. 1.) All the J vs. τ plots will be presented on exactly the same scale. Thus, there are 22 figures for ln J vs. ln τ like fig. 1 and they all have the same scale and span the same ranges in J and τ.

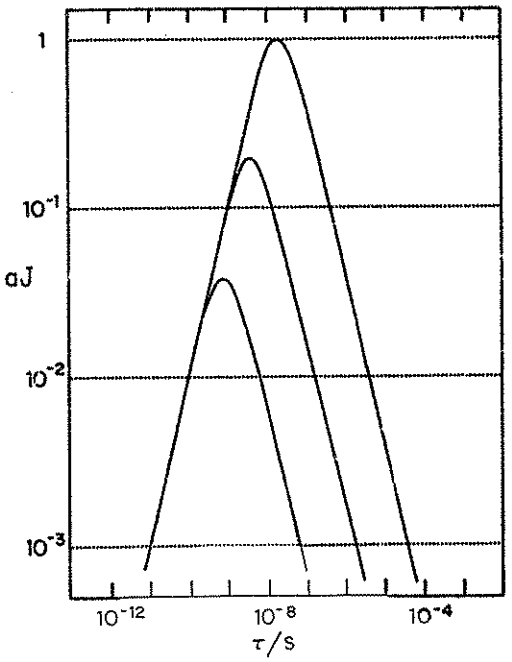

Fig. 1. Log–log plot of $aJ_{BPP}(\omega, \tau)$ vs. unique correlation time τ at Larmor frequencies of $\omega/(2\pi) = 8$ (top), 40 (middle), and 200 MHz (bottom). The Bloembergen–Purcell–Pound or δ-function (BPP) spectral density J_{BPP} results from Poisson statistics which implies a single correlation time. The normalization $a = \omega_1^{-1} = [(2\pi)\ 8\ \text{MHz}]^{-1}$ such that $J_{BPP,\,max} = 1$ at 8 MHz.

This will allow direct comparisons between the different spectral densities. This format does not rely on a specific relationship between the correlation time and other parameters such as temperature or pressure. At the same time, however, if an Arrhenius relationship for τ is assumed (see ahead to eq. (45)), $\ln \tau$ becomes a reduced inverse temperature scale, normalized by the effective activation temperature E/k. Figure 1 shows the frequency dependence of J_{BPP} vs. τ by plotting ln J vs. ln τ at three angular frequencies, $\omega_1 = 2\pi(8\,\mathrm{MHz})$, $\omega_2 = 2\pi(40\,\mathrm{MHz})$ and $\omega_3 = 2\pi(200\,\mathrm{MHz})$. For plotting purposes, we have chosen a normalization a for all the spectral densities such that $aJ_{\mathrm{BPP,\,max}} = 1$ for ω_1. It follows from eq. (26) that the parameter a (where aJ rather than J is plotted) is $a = \omega_1^{-1}$. The other two frequencies are $\omega_2 = 5\omega_1$ and $\omega_3 = 5\omega_2 = 25\omega_3$. These three frequencies are convenient for displaying the frequency dependence of all the spectral densities but the range also corresponds to convenient and practical choices for the experimentalist. Frequencies above 200 MHz for solid state NSR studies are available but the instruments for work with solids are expensive to purchase and they tend to be expensive and time consuming to run (only in practice, not in principle). A more important aspect is that for most motions studied by solid state NSR, observed relaxation rates become very small at high frequencies, thus the experiments are intrinsically very time consuming and there is often little to be gained since J_{max} for Zeeman relaxation rates will usually occur at too high a temperature (i.e., too small a τ, see fig. 1). At low frequencies, signal-to-noise becomes a problem as does the recovery of the amplifier-detection system. (See [87] for a complete discussion of the art of doing pulsed nuclear magnetic resonance experiments.) For solid state NMR, these problems are very serious below about 4 MHz. Although measurements of Zeeman relaxation rates are the best and most direct way of learning about the spectral density, they do have these frequency limitations. Motions of much lower frequencies are studied either by field cycling techniques [113] or by measuring dipolar order or rotating frame relaxation rates as discussed in section 3.2. However, in the analysis of experimental data, separating the zero (dipolar) or low frequency (rotating frame) components from the ω_0 (and usually $2\omega_0$) component can be difficult. In fitting experimental Zeeman relaxation data, it is very important to observe at least three frequencies and to observe both the long and short correlation time regimes ($\omega\tau \gg 1$ and $\omega\tau \ll 1$ respectively) in order to characterize the spectral density. As will be seen, a frequency-independent short correlation time limit such as that displayed in fig. 1, is common to several spectral densities and only by measuring at several frequencies can certain spectral densities be distinguished from one another. Also, in a plot of ln J vs. ln τ, several spectral densities have equal and opposite (constant) slopes for small and large τ and, again, only by observing at several frequencies can the spectral densities be distinguished from one another.

6.2. *Bloembergen–Purcell–Pound or δ-function (BPP)*

The distribution $\Lambda(\xi)$ is

$$\Lambda_{\mathrm{BPP}}(\xi, \tau) = \delta(\xi - \tau)\,, \tag{41}$$

where $\delta(x)$ is a Dirac δ-function. Equation (35) then gives eq. (26) for J_{BPP} [57, 59]. Ln J_{BPP} vs. ln τ for the three frequencies is plotted in fig. 1; it has the limiting values

$$J_{\mathrm{BPP}}(\omega, \tau) = 2\tau\,, \quad \omega\tau \ll 1\,; \tag{42}$$

and

$$J_{\mathrm{BPP}}(\omega, \tau) = 2\tau^{-1}\omega^{-2}\,, \quad \omega\tau \gg 1\,; \tag{43}$$

and the maximum value

$$J_{\mathrm{BPP,\,max}} = \omega^{-1}, \quad \omega\tau = 1. \tag{44}$$

The small and large τ regimes (i.e., $\omega\tau \ll 1$ and $\omega\tau \gg 1$) of $\ln J$ vs. $\ln \tau$ in fig. 1 are characterized by slopes of +1 (eq. 42) and −1 (eq. 43), respectively. Experimentally this corresponds to the high and low temperature regimes, respectively, and if an Arrhenius relationship.

$$\tau = \tau_\infty \exp(E/kT) \tag{45}$$

is assumed and if T^{-1} rather than $\ln \tau$ is plotted on the horizontal axis, the slopes are $+E/k$ and $-E/k$.

6.3. *Havriliak–Negami (HN)*

Dissado and Hill (DH) have developed a very general dielectric relaxation (DR) spectral density [90, 91] which successfully interprets very many sets of DR data [114]. It has also been used to interpret mechanical relaxation data [115]. The dynamical model [90, 91, 116] on which the DH spectral density is based assumes both distributions of motional barriers and the presence of correlated motions. There is an asymmetric anisotropic potential and the many-body problem is introduced via a distribution of well depths. This distribution is characterized by a parameter n where $0 < n < 1$. The value of n depends on the details of the averaging procedure and is material-dependent. A value of $n = 0$ corresponds to a unique barrier height and a value of $n = 1$ corresponds to the greatest allowed distribution of barrier heights. Correlated motions among the dipoles will effect the relaxation and this is characterized by a parameter m, $0 < m < 1$ where $m = 1$ corresponds to no correlated motions and $m = 0$ corresponds to perfectly correlated motions.

The DH spectral density $H(\omega)$ for this model [90, 91] requires numerical evaluation of confluent hypergeometric functions. It is often preferable and more convenient to deal with simpler algebraic functions if possible and we note, as previously pointed out [117], that the phenomenological spectral density due to Havriliak and Negami (HN) [118] has many properties in common with the DH spectral density although it is different in appreciable ways [119]. The HN DR spectral density is

$$H_{\mathrm{HN}}(\omega) = [1 + (\mathrm{i}\omega/\omega_{\mathrm{p}})^{\delta}]^{-\varepsilon}, \tag{46}$$

where $0 < \delta < 1$ and $\varepsilon < \delta^{-1}$. This reduces to the Debye spectral density in eq. (34) when $\varepsilon = \delta = 1$. Although there is no fundamental theoretical relationship between the microscopic fundamental parameter pair m, n in the DH model and the phenomenological parameter pair δ, ε in the HN model, they can be related by fitting the same relaxation data. The relationship is $m = \delta$ and $n = 1 - \delta\varepsilon$. Thus, δ is a measure of the correlations and the product $\delta\varepsilon$ is a measure of a spread in barriers. The NSR $J(\omega)$ is obtained from eq. (33) and is

$$J_{\mathrm{HN}}(\omega, \tau, \varepsilon, \delta) = \frac{2}{\omega} \sin\left[\varepsilon \arctan\left\{\frac{(\omega\tau)^{\delta} \sin(\delta\pi/2)}{1 + (\omega\tau)^{\delta} \cos(\delta\pi/2)}\right\}\right]$$

$$\times [1 + 2(\omega\tau)^{\delta} \cos(\delta\pi/2) + (\omega\tau)^{2\delta}]^{-\varepsilon/2}, \tag{47}$$

where we set $\tau = \omega_p^{-1}$. That is, we associate a characteristic NSR correlation time τ with the inverse of the peak loss frequency ω_p. To tie this in with the more general framework discussed previously, $x_1 = \tau$, $x_2 = \varepsilon$ and $x_3 = \delta$ in eq. (35). Ln J_{HN} vs. ln τ for $\omega/(2\pi) = 8$, 40 and 200 MHz is shown in fig. 2 for $\varepsilon = 0.5$ and $\delta = 0.5$. Ln J_{HN} vs. ln τ for $\delta = 0.5$ and several values of ε is shown in fig. 3 and ln J_{HN} vs. ln τ for $\varepsilon = 0.2$ and several values of δ is shown in fig. 4. As in all cases where the dependence of J on a particular parameter other than ω is being shown, we choose the middle frequency, $\omega_2 = (2\pi)40$ MHz. This allows for direct comparison between the manner in which various spectral densities depend on their parameters. Note that the $\varepsilon = \delta = 0.5$ plot is common to figs. 2 and 3 and that the $\varepsilon = 0.2$, $\delta = 0.5$ plot is common to figs. 3 and 4. Since we are really showing two dimensional projections of multi-dimensional spaces, it is convenient to make these kinds of comparisons. This can be done throughout this paper.

At high temperatures where τ is sufficiently small that $\omega\tau \ll 1$, J reduces to

$$J_{HN}(\omega, \tau, \varepsilon, \delta) = 2\varepsilon[\sin(\delta\pi/2)]\tau^{\delta}\omega^{-(1-\delta)} \tag{48}$$

and at low temperatures where $\omega\tau \gg 1$,

$$J_{HN}(\omega, \tau, \varepsilon, \delta) = 2[\sin(\varepsilon\delta\pi/2)]\tau^{-\delta\varepsilon}\omega^{-(1+\delta\varepsilon)}. \tag{49}$$

The HN spectral density reduces to the Cole–Cole spectral density (section 6.4) if $\varepsilon = 1$ and to the Davidson–Cole spectral density (section 6.5) if $\delta = 1$.

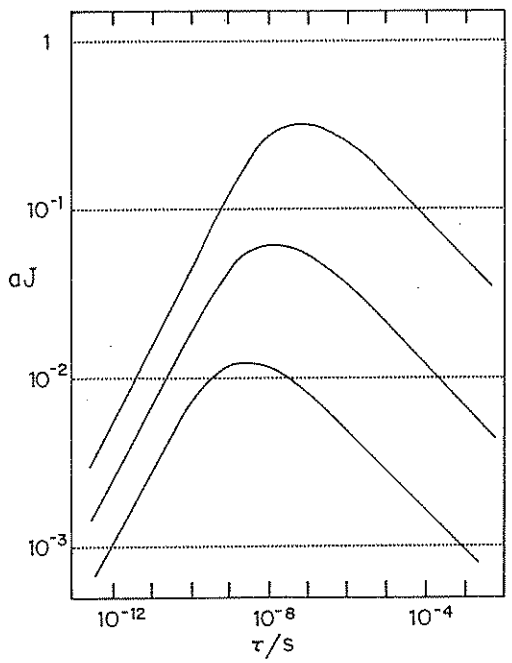

Fig. 2. Log–log plot of $aJ_{HN}(\omega, \tau, \varepsilon, \delta)$ vs. characteristic correlation time τ for $\varepsilon = 0.5$ and $\delta = 0.5$ at Larmor frequencies of $\omega/(2\pi) = 8$ (top), 40 (middle) and 200 MHz (bottom). J_{HN} is the Havriliak–Negami spectral density. The normalization $a = \omega_1^{-1} = [(2\pi)\ 8\,\text{MHz}]^{-1}$ such that $J_{BPP,\,max} = 1$ at 8 MHz.

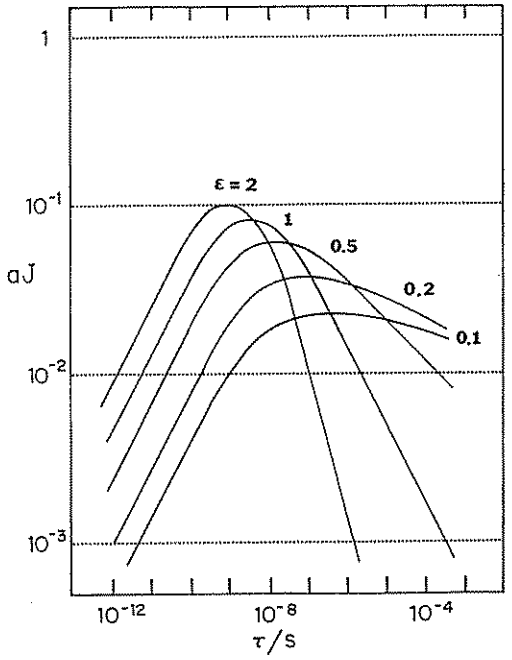

Fig. 3. Log–log plot of $aJ_{HN}(\omega, \tau, \varepsilon, \delta)$ vs. characteristic correlation time τ at the Larmor frequency $\omega/(2\pi) = 40$ MHz and $\delta = 0.5$ for several values of ε as shown. J_{HN} is the Havriliak–Negami spectral density. The normalization $a = \omega_1^{-1} = [(2\pi)\ 8\,\text{MHz}]^{-1}$ such that $J_{BPP,\,max} = 1$ at 8 MHz.

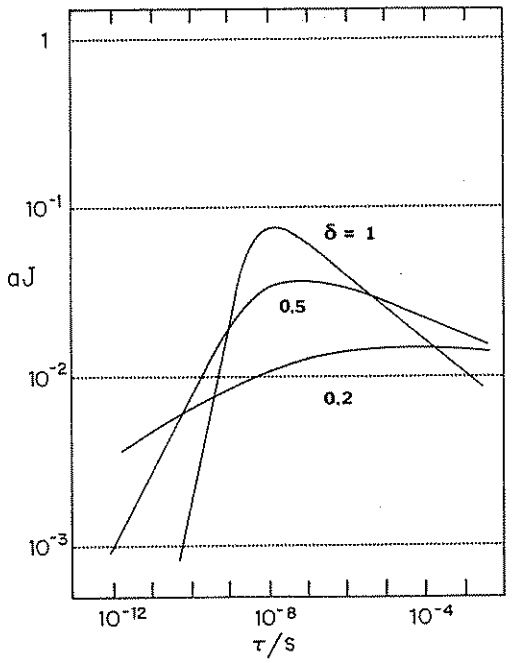

Fig. 4. Log–log plot of $aJ_{HN}(\omega, \tau, \varepsilon, \delta)$ vs. characteristic correlation time τ at the Larmor frequency $\omega/(2\pi) = 40$ MHz and $\varepsilon = 0.2$ for three values of δ as shown. J_{HN} is the Havriliak–Negami spectral density. The normalization $a = \omega_1^{-1} = [(2\pi)\ 8\,\text{MHz}]^{-1}$ such that $J_{BPP,\,max} = 1$ at 8 MHz.

The HN spectral density fits DR data [120] in a way which, in some cases, mimics the spectral density obtained from using, in eq. (24), the non-exponential correlation function $G(t) = \exp\{-(t/\tau)^{\beta}\}$ introduced by Kohlrausch [121] and first used by Williams and Watts in DR studies [122]. This KWW correlation function has been discussed extensively [123–128].

6.4. *Cole–Cole (CC)*

The Cole–Cole (CC) DR spectral spectral density can be arrived at from a distribution of Debye spectral densities [129]. The distribution $\theta_{CC}(z, \varepsilon)$ defined in eq. (40) is

$$\theta_{CC}(z, \delta) = \frac{1}{2\pi}\sin(\delta\pi)\left[\frac{1}{\cosh(\delta z) + \cos(\delta\pi)}\right], \tag{50}$$

with $0 < \delta \leq 1$, and it is plotted in fig. 5 for $\delta = 0.5$ (the larger of the two plots at $z = 0$) and $\delta = 0.2$. The parameter δ characterizes the width of the distribution. The independent variable z used in fig. 5 is, again, introduced via eq. (40) and is $z = \ln(\xi/\tau)$ where τ is the correlation time corresponding to the maximum of θ_{CC} or Λ_{CC}.

The NSR spectral density is given by eq. (33) with $H(\omega)$ given by CC [129]. Equivalently, it is obtained from the HN spectral density in eq. (47) with $\varepsilon = 1$. Finally, it is also obtained by substituting the distribution in eq. (50) into eq. (35) via eq. (40). In the context of the microscopic DH model (with $\varepsilon = 1$) the parameter $\delta = m = 1 - n$ is a measure of the degree of correlated motion as well as the distribution of correlation times (activation energies). $\delta = 1$ implies a unique activation energy and no correlated motion whereas $\delta = 0$ implies the maximum distribution of activation energies and a

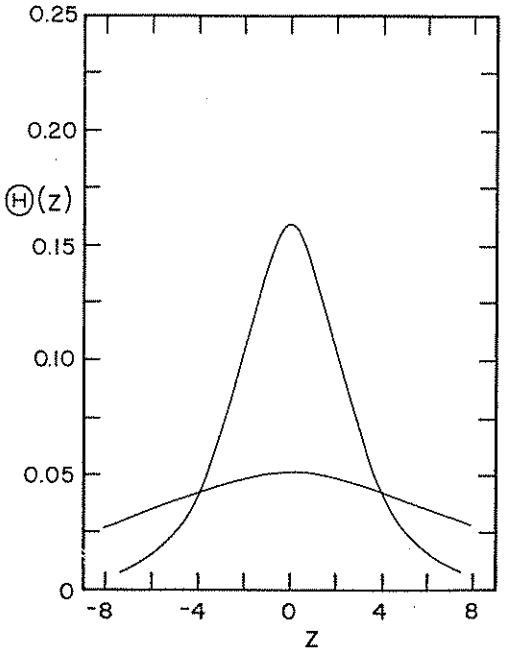

Fig. 5. $\theta_{CC}(z, \delta)$ vs. z for $\delta = 0.5$ (top) and 0.2 (bottom). The Cole–Cole (CC) distribution $A_{CC}(\xi, \tau, \delta)$ of correlation times ξ is characterized by $\theta_{CC}(z, \delta)$ with $z = \ln(\xi/\tau)$ for characteristic correlation time τ and width parameter δ.

considerable degree of correlated motion. The spectral density is

$$J_{CC}(\omega, \tau, \delta) = \frac{2}{\omega} \sin\left(\frac{\delta\pi}{2}\right)\left[\frac{(\omega\tau)^{\delta}}{1 + (\omega\tau)^{2\delta} + \{2\cos(\delta\pi/2)\}(\omega\tau)^{\delta}}\right]. \tag{51}$$

Ln J_{CC} vs. ln τ for the three frequencies is shown in fig. 6 for $\delta = 0.5$ and ln J_{CC} vs. ln τ for various values of δ at $\omega/(2\pi) = 40$ MHz is shown in fig. 7. In fig. 7, the case of $\delta = 1$ for J_{CC} vs. τ is identical to the middle plot of fig. 1 for J_{BPP} vs. τ (since $J_{CC} \rightarrow J_{BPP}$ as $\delta \rightarrow 1$) and the case of $\delta = 0.5$ in fig. 7 is identical to the middle plot of fig. 6. The $\omega\tau \ll 1$ and $\gg 1$ limits are

$$J_{CC}(\omega, \tau, \delta) = 2[\sin(\delta\pi/2)]\tau^{\delta}\omega^{-(1-\delta)}, \quad \omega\tau \ll 1; \tag{52}$$

and

$$J_{CC}(\omega, \tau, \delta) = 2[\sin(\delta\pi/2)]\tau^{-\delta}\omega^{-(1+\delta)}, \quad \omega\tau \gg 1; \tag{53}$$

and the slopes of ln J_{CC} vs. ln τ in the two regimes are $+\delta$ and $-\delta$. The maximum value of J_{CC} depends on both ω and δ and is given by

$$J_{CC,\,max} = \frac{1}{\omega}\left[\frac{\sin(\delta\pi/2)}{1 + \cos(\delta\pi/2)}\right], \quad \omega\tau = 1. \tag{54}$$

The CC spectral density has been used extensively in DR studies [85, 129] and has found limited use in NSR studies [130].

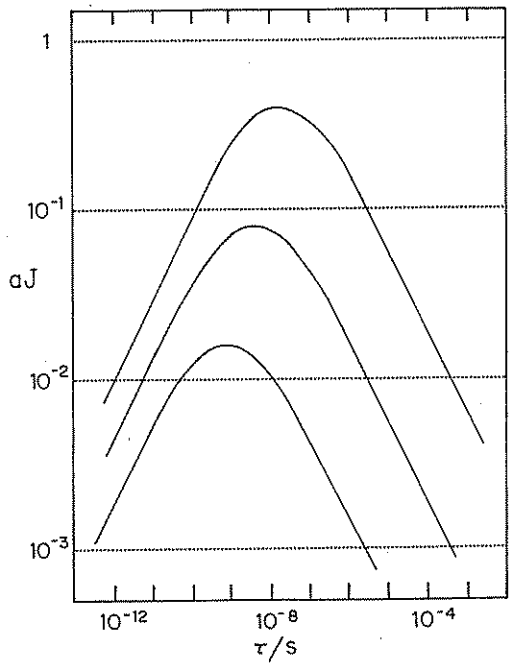

Fig. 6. Log–log plot of $aJ_{CC}(\omega, \tau, \delta)$ vs. characteristic correlation time τ for width parameter $\delta = 0.5$ at Larmor frequencies of $\omega/(2\pi) = 8$ (top), 40 (middle) and 200 MHz (bottom). The spectral density J_{CC} results from a Cole–Cole distribution of correlation times or, equivalently, it follows from the Havriliak–Negami spectral density with $\varepsilon = 1$. The value of δ used here is the same as that used to generate the top distribution in fig. 5. The normalization $a = \omega_1^{-1} = [(2\pi)\ 8\,\text{MHz}]^{-1}$ such that $J_{BPP,\,max} = 1$ at 8 MHz.

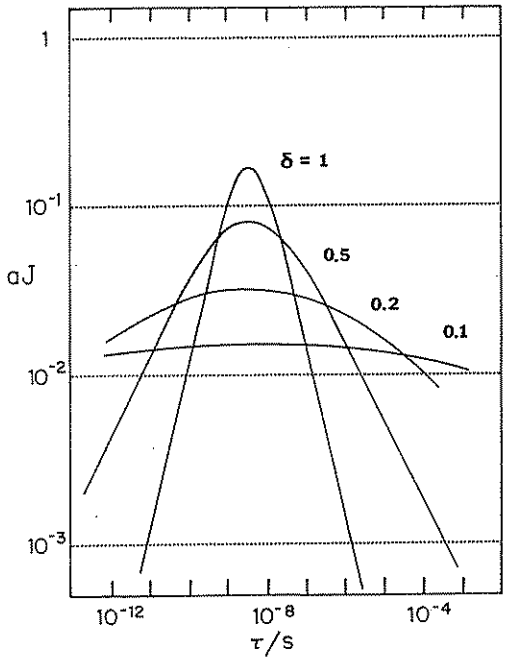

Fig. 7. Log–log plot of $aJ_{CC}(\omega, \tau, \delta)$ vs. characteristic correlation time τ at the Larmor frequency $\omega/(2\pi) = 40$ MHz for several width parameters δ as shown. The spectral density J_{CC} results from a Cole–Cole distribution of correlation times or, equivalently, it follows from the Havriliak–Negami spectral density with $\varepsilon = 1$. Two of the δ values (0.5 and 0.2) used here are the same as those used to generate the two distributions in fig. 5. The normalization $a = \omega_1^{-1} = [(2\pi)\ 8\,\text{MHz}]^{-1}$ such that $J_{BPP,\,max} = 1$ at 8 MHz.

6.5. *Davidson–Cole (DC)*

The spectral density due to Davidson and Cole [131] is one of the most successful spectral densities used to interpret nuclear spin relaxation experiments in solids [37, 60, 132–137]. it follows from the HN spectral density in eq. (47) by setting $\delta = 1$ and, as such, the DC spectral density can mimic the KWW spectral density under certain conditions (see section 6.3). Equivalently, it comes from a distribution of correlation parameters z given by;

$$\theta_{DC}(z, \varepsilon) = \frac{\sin(\varepsilon\pi)}{\pi}\left(\frac{1}{e^{-z} - 1}\right)^{\varepsilon}, \quad z < 0;$$
$$= 0, \qquad z \geq 0; \tag{55}$$

with $0 < \varepsilon \leq 1$. This distribution function follows if the DR spectral density $H(\omega)$ is taken as $1/(1 + i\omega\tau)^{\varepsilon}$ with $0 < \varepsilon \leq 1$ rather than the Debye case of $\varepsilon = 1$ (which leads to the BPP spectral density). The distribution function $F(y)$ with $y = \xi/\tau$ used by DC in their original work [131] is related to the forms used here by $F(y)\,\mathrm{d}[\ln(y)] = \Delta(y)\,\mathrm{d}y = \Lambda(\xi)\,\mathrm{d}\xi = \theta(z)\,\mathrm{d}z$ so $F(y)$ in DC is different from the $\Delta(y)$ in eq. (38). The cutoff value of $z = 0$ corresponds to the correlation time $\xi = \tau$. For the DC distribution, the characteristic correlation time τ is called the upper cutoff correlation time.

$\theta_{DC}(z, \varepsilon)$ vs. z is shown in fig. 8 for $\xi = 0.5$, 0.2 and 0.1. (Note that all six θ vs. z plots in this paper have the same scale.) $\theta(z) \to \infty$ as $z \to 0$ or, equivalently, $\Lambda(\xi) \to \infty$ as $\xi \to \tau$. Also, $\Lambda(\xi) \to \delta(\tau - \xi)$ or $\theta(z) \to \delta(0)$ as $\varepsilon \to 1$. The case of $z = 0$ $(\xi = \tau)$ might correspond to the correlation time for a unit (whole molecular or intramolecular rotor) in the perfect crystalline structure. If there are crystal imperfections, the result might be to create a variety of environments for the unit, all of which lead to smaller barriers and therefore to shorter ξ values.

Within the framework of the DH DR theory, $\delta = m = 1$, $\varepsilon = 1 - n \neq 1$ implies no correlated motions but a distribution of activation energies and therefore a distribution of correlation times. Thus, the original phenomenological development of the DC spectral density is consistent with the more recent microscopic theory of DH. Also, whereas many DR studies involve very large molecules (polymers) where correlated motions are expected to be important, many NSR studies involve simpler systems where one might not expect correlated motions. Thus it is understandable and encouraging that the DC spectral density has extensive applications in NSR studies of simple molecules.

The DC spectral density is

$$J_{DC}(\omega, \tau, \varepsilon) = \frac{2}{\omega} \left\{ \frac{\sin[\varepsilon \arctan(\omega\tau)]}{(1 + \omega^2\tau^2)^{\varepsilon/2}} \right\}. \tag{56}$$

Ln J_{DC} vs. ln τ for the three frequencies is shown in figs. 9 and 10 for $\varepsilon = 0.5$ and 0.1 respectively. Ln J_{DC} vs. ln τ for various values of ε is shown in fig. 11. For $\omega\tau \ll 1$ and $\omega\tau \gg 1$, J_{DC} is

$$J_{DC}(\omega, \tau, \varepsilon) = 2\varepsilon\tau\,, \quad \omega\tau \ll 1\,; \tag{57}$$

and

$$J_{DC}(\omega, \tau, \varepsilon) = 2[\sin(\varepsilon\pi/2)]\tau^{-\varepsilon}\omega^{-(1+\varepsilon)}\,, \quad \omega\tau \gg 1\,. \tag{58}$$

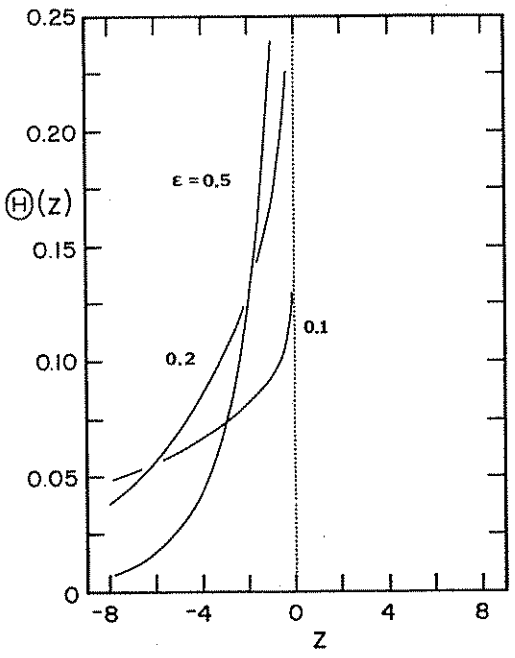

Fig. 8. $\theta_{DC}(z, \varepsilon)$ vs. z for $\varepsilon = 0.5$, 0.2 and 0.1 as shown. The Davidson–Cole (DC) distribution $\Lambda_{DC}(\xi, \tau, \varepsilon)$ of correlation times ξ is characterized by $\theta_{DC}(z, \varepsilon)$ with $z = \ln(\xi/\tau)$ for upper cutoff correlation time τ and width parameter ε.

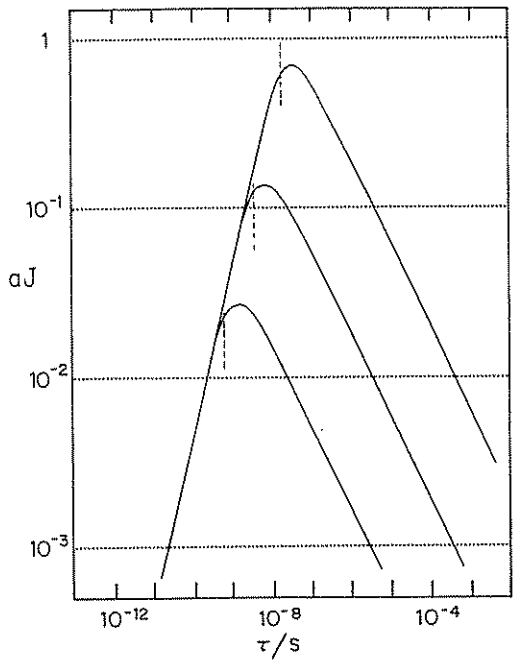

Fig. 9. Log–log plot of $aJ_{DC}(\omega, \tau, \varepsilon)$ vs. upper cutoff correlation time τ for width parameter $\varepsilon = 0.5$ at Larmor frequencies of $\omega/(2\pi) = 8$ (top), 40 (middle) and 200 MHz (bottom). The vertical dashed lines indicate the values $\tau = \omega^{-1}$. The spectral density J_{DC} results from a Davidson–Cole distribution of correlation times or, equivalently, it follows from the Havriliak–Negami spectral density with $\delta = 1$. The value of ε used here is the same as that used to generate the narrowest of the three distributions in fig. 8. The normalization $a = \omega_1^{-1} = [(2\pi)\ 8\,\text{MHz}]^{-1}$ such that $J_{BPP,\,max} = 1$ at 8 MHz.

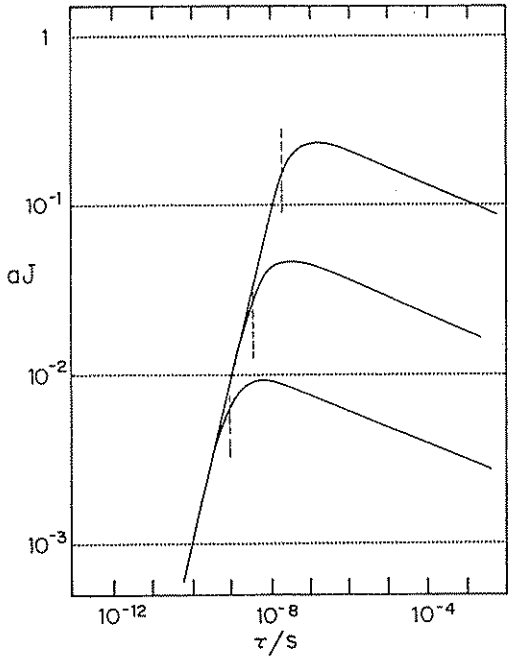

Fig. 10. Log–log plot of $aJ_{DC}(\omega, \tau, \varepsilon)$ vs. upper cutoff correlation time τ for width parameter $\varepsilon = 0.1$ at Larmor frequencies of $\omega/(2\pi) = 8$ (top), 40 (middle) and 200 MHz (bottom). The vertical dashed lines indicate the values $\tau = \omega^{-1}$. The spectral density J_{DC} results from a Davidson–Cole distribution of correlation times or, equivalently, it follows from the Havriliak–Negami spectral density with $\delta = 1$. The value of ε used here is the same as that used to generate the widest of the three distributions in fig. 8. The normalization $a = \omega_1^{-1} = [(2\pi)\ 8\,\text{MHz}]^{-1}$ such that $J_{BPP,\,max} = 1$ at 8 MHz.

The $\omega\tau \ll 1$ slope of $\ln J_{DC}$ vs. $\ln \tau$ is 1 and the $\omega\tau \gg 1$ slope is $-\varepsilon$. Unlike the Fuoss–Kirkwood spectral density J_{FK} (section 6.7) and J_{CC} (section 6.4) but like J_{BPP} (section 6.2), the $\omega\tau \ll 1$ regime is frequency independent and NSR experiments at high temperatures could not distinguish between J_{BPP} and J_{DC}. At low temperatures ($\omega\tau \gg 1$), $J_{DC} \propto \omega^{-1-\varepsilon}$ (with $\varepsilon = 1$ giving the $J_{BPP} \propto \omega^{-2}$ result). The maximum value of J_{DC} satisfies the condition

$$(\omega\tau)\tan[\varepsilon \arctan(\omega\tau)] = 1\,. \tag{59}$$

$J_{DC,\,max}$ for several values of ε can be seen in fig. 11. As ε goes from 1 to 0, the value $\omega\tau$ at which $J_{DC,\,max}$ occurs goes from 1 to ∞. As a benchmark, the value of $\tau = \omega^{-1}$ is indicated by the vertical dashed lines in figs. 9 and 10. In fig. 11 where all plots correspond to the same frequency, this $\tau = \omega^{-1}$ occurs at the position of the peak for the $\varepsilon = 1$ curve.

The DC spectral density is discussed further in sections 6.6 and 6.8.

6.6. *Fang (FAN)*

The FAN spectral density [138] comes from a distribution function $\theta_{FAN}(z)$ which is the mirror image (about $z = 0$) of $\theta_{DC}(z)$ shown in fig. 8 so we use the same symbol ε for the distribution parameter. Like

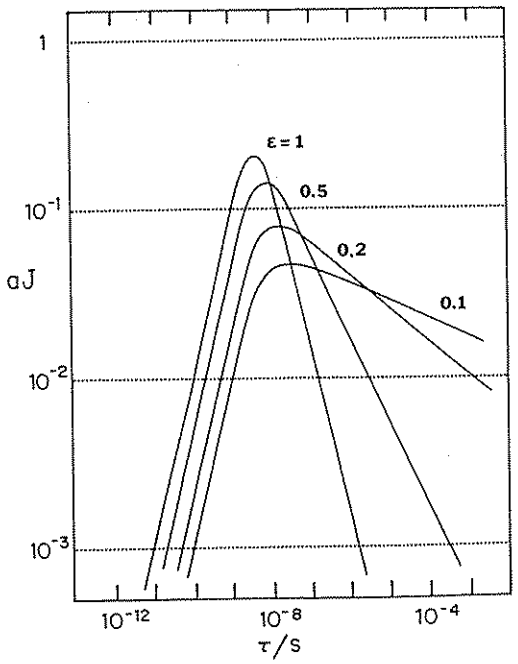

Fig. 11. Log–log plot of $aJ_{DC}(\omega, \tau, \varepsilon)$ vs. upper cutoff correlation time τ at the Larmor frequency $\omega/(2\pi) = 40$ MHz for several width parameters ε as shown. The spectral density J_{DC} results from a Davidson–Cole distribution of correlation times or, equivalently, it follows from the Havriliak–Negami spectral density with $\delta = 1$. The values of $\varepsilon = 0.5$, 0.2 and 0.1 used here are the same as those used to generate the three distributions in fig. 8 and the plot corresponding to the value of $\varepsilon = 1$ is identical to the middle J_{BPP} plot in fig. 1. The normalization $a = \omega_1^{-1} = [(2\pi)\ 8\ \text{MHz}]^{-1}$ such that $J_{BPP,\,max} = 1$ at 8 MHz.

the DC case, $\xi = \tau$ (now called the lower cutoff correlation time) might again correspond to the perfect crystalline environment, only now all imperfections lead to more hindered environments and therefore larger correlation times. $\theta_{FAN}(z)$ arises from assuming that the normalized complex dielectric susceptibility is of the form $H(\omega) = (i\omega\tau)^{\varepsilon}/(1 + i\omega\tau)^{\varepsilon}$ [138] and is given by

$$\theta_{FAN}(z, \varepsilon) = \frac{\sin(\varepsilon\pi)}{\pi}\left(\frac{1}{e^{z} - 1}\right)^{\varepsilon}, \quad z > 0;$$
$$= 0, \qquad\qquad z \leq 0; \tag{60}$$

with $0 < \varepsilon \leq 1$. The NSR spectral density is

$$J_{FAN}(\omega, \tau, \varepsilon) = \frac{2(\omega\tau)^{\varepsilon}}{\omega}\left\{\frac{\sin[\varepsilon\ \text{arccot}(\omega\tau)]}{(1 + \omega^2\tau^2)^{\varepsilon/2}}\right\}. \tag{61}$$

Ln J_{FAN} vs. ln τ for the three frequencies is shown in fig. 12 for $\varepsilon = 0.1$. The low and high τ limits are

$$J_{FAN}(\omega, \tau, \varepsilon) = 2[\sin(\varepsilon\pi/2)](1 - \varepsilon)^{-1}\tau^{\varepsilon}, \quad \omega\tau \ll 1; \tag{62}$$

$$J_{FAN}(\omega, \tau, \varepsilon) = 2\varepsilon\tau^{-1}\omega^{-2}, \qquad \omega\tau \gg 1. \tag{63}$$

The ln J_{FAN} vs. ln τ slope is ε for $\omega\tau \ll 1$ and -1 for $\omega\tau \gg 1$. This is just the opposite from J_{DC}.

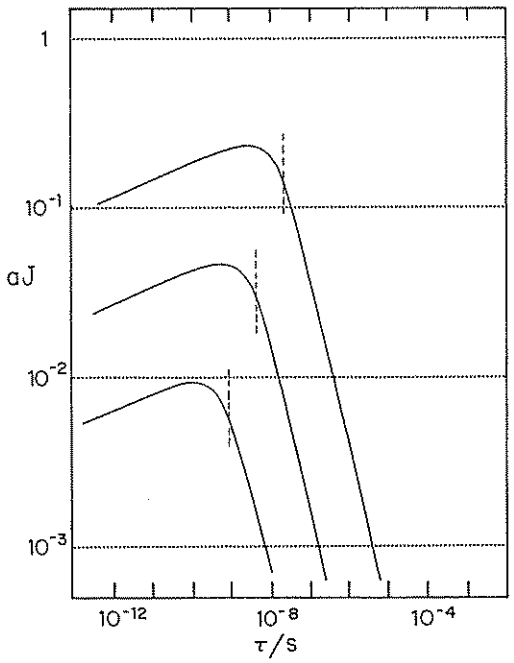

Fig. 12. Log–log plot of $aJ_{FAN}(\omega, \tau, \varepsilon)$ vs. lower cutoff correlation time τ for width parameter $\varepsilon = 0.1$ at Larmor frequencies of $\omega/(2\pi) = 8$ (top), 40 (middle) and 200 MHz (bottom). The vertical dashed lines indicate the values $\tau = \omega^{-1}$. The spectral density J_{FAN} results from a Fang distribution of correlation times. This value of ε corresponds to a distribution of correlation times given by the mirror image of the $\varepsilon = 0.1$ curve about the vertical dotted line in fig. 8. The normalization $a = \omega_1^{-1} = [(2\pi)\,8\,\text{MHz}]^{-1}$ such that $J_{BPP,\,max} = 1$ at 8 MHz.

$J_{DC} = \varepsilon J_{BPP}$ for $\omega\tau \ll 1$ whereas $J_{FAN} = \varepsilon J_{BPP}$ for $\omega\tau \gg 1$. At a single frequency, J_{DC} and J_{FAN} are mirror images with the mirror at $\tau = \omega^{-1}$. Thus, the plots at each frequency in figs. 10 and 12 are mirror images about the indicated vertical lines, yet the frequency dependence of the two spectral densities is quite different. We note that a spectral density with the high temperature (small τ) slope less than the low temperature (large τ) slope occurs for a rotor with different well depths [139–142] but the frequency dependence is quite different from that presented here. It is imperative in any relaxation experiment to do a frequency study. The maximum value of J_{FAN} satisfies the condition

$$(\omega\tau)\cot[\varepsilon\,\text{arccot}(\omega\tau)] = (\omega\tau)^2 - \omega\tau + 1\,. \tag{64}$$

As ε goes from 1 to 0, the value of $\omega\tau$ at which $J_{FAN,\,max}$ occurs goes from 1 to 0 as opposed to from 1 to ∞ as in the DC case.

Some interesting general features of the DC and FAN spectral densities, including their relationship, have been discussed elsewhere [143]. To our knowledge, J_{FAN} has not been used to interpret NSR experiments but because θ_{FAN} is the mirror image of θ_{DC}, and both are physically reasonable, it merits investigation.

6.7. *Fuoss–Kirkwood (FK)*

The distribution of correlation times due to FK [144] again has its origin in the interpretation of DR rates [85, 144]. It has also been used in an incoherent neutron scattering study [145] but to our knowledge it has not been used successfully to interpret NSR data. The distribution of correlation

parameters z is given by

$$\theta_{FK}(z, \beta) = \left[\frac{\beta \cos(\beta\pi/2)}{\pi}\right]\left[\frac{\cosh(\beta z)}{\sinh^2(\beta z) + \cos^2(\beta\pi/2)}\right], \tag{65}$$

with $0 < \beta \leq 1$. Here, τ is the characteristic correlation time (namely the value of ξ at which both the asymmetric distribution $\Lambda_{FK}(\xi, \tau, \beta)$ and the symmetric distribution $\theta_{FK}(z, \beta)$ have their maximum values) and β characterizes the width of Λ_{FK} and θ_{FK}. The (symmetric) distribution $\theta_{FK}(z)$ is shown in fig. 13 for $\beta = 0.5$ (the narrower of the two) and 0.2 (the wider of the two). As $\beta \to 1$, $\theta(z) \to \delta(0)$ or, equivalently, $\Lambda(\xi) \to \delta(\xi - \tau)$ as required. Thus as $\beta \to 1$, $J_{FK} \to J_{BPP}$. The spectral density is obtained using eqs. (40) and (65) in eq. (35). The somewhat involved mathematics is done thoroughly by FK [144]. $J(\omega)$ corresponds to $(2/\omega)$ times the imaginary part of the "reduced polarization" used by FK [144] (the DR normalized spectral density $H(\omega)$ in eq. (32)). The NSR spectral density is given by

$$J_{FK}(\omega, \tau, \beta) = \frac{2\beta}{\omega}\left[\frac{(\omega\tau)^{\beta}}{1 + (\omega\tau)^{2\beta}}\right]. \tag{66}$$

Ln J_{FK} vs. ln τ for the three frequencies is shown in fig. 14 for $\beta = 0.5$ and ln J_{FK} vs. ln τ for several

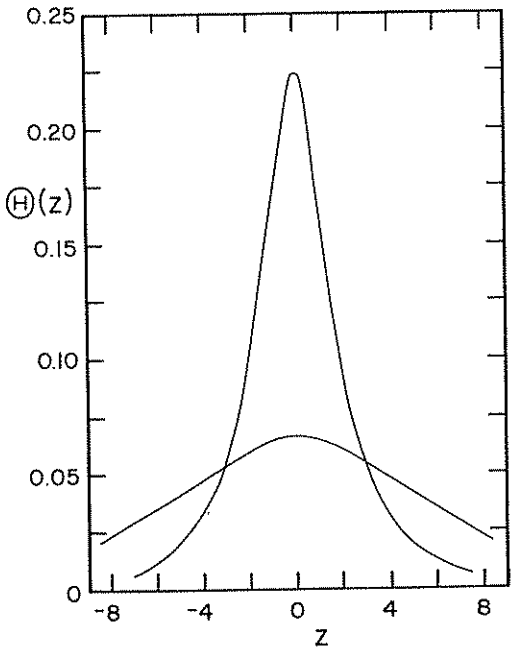

Fig. 13. $\theta_{FK}(z, \beta)$ vs. z for $\beta = 0.5$ (top) and 0.2 (bottom). The Fuoss–Kirkwood (FK) distribution $\Lambda_{FK}(\xi, \tau, \beta)$ of correlation times ξ is characterized by $\theta_{FK}(z, \beta)$ with $z = \ln(\xi/\tau)$ for characteristic correlation time τ and width parameter β.

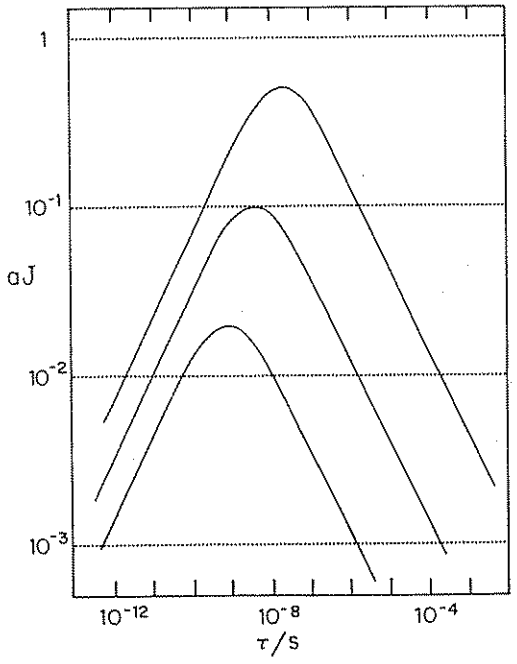

Fig. 14. Log–log plot of $aJ_{FK}(\omega, \tau, \varepsilon)$ vs. characteristic correlation time τ for width parameter $\beta = 0.5$ at Larmor frequencies of $\omega/(2\pi) = 8$ (top), 40 (middle) and 200 MHz (bottom). The spectral density J_{FK} results from a Fuoss–Kirkwood distribution of correlation times. The value of β used here is the same as that used to generate the top curve in fig. 13. The normalization $a = \omega_1^{-1} = [(2\pi)\,8\,\text{MHz}]^{-1}$ such that $J_{BPP,\,max} = 1$ at 8 MHz.

values of β is shown in fig. 15. The short and long correlation time limits are

$$J_{\mathrm{FK}}(\omega, \tau, \beta) = 2\beta\tau^{\beta}\omega^{-(1-\beta)}, \quad \omega\tau \ll 1; \tag{67}$$

and

$$J_{\mathrm{FK}}(\omega, \tau, \beta) = 2\beta\tau^{-\beta}\omega^{-(1+\beta)}, \quad \omega\tau \gg 1; \tag{68}$$

and the value of $J_{\max}$ is

$$J_{\mathrm{FK,\,max}} = \beta\omega^{-1}, \quad \omega\tau = 1. \tag{69}$$

The ratio

$$J_{\mathrm{FK,\,max}}/J_{\mathrm{BPP,\,max}} = \beta. \tag{70}$$

The frequency dependence of J_{FK} in the $\omega\tau \ll 1$ and $\omega\tau \gg 1$ limits is $\omega^{1-\beta}$ and $\omega^{1+\beta}$ and the low and high $\omega\tau$ slopes of ln J_{FK} vs. ln τ are $+\beta$ and $-\beta$. In terms of experimental results, this would be $+\beta E/k$ and $-\beta E/k$ if eq. (45) with constant τ_∞ were used for τ and if T^{-1} replaced ln τ on the horizontal axis.

Since the large and small τ limiting slopes of J vs. τ are the same for the BPP, FK and CC spectral densities, if data is taken at only one frequency and the value of $R_{\max}$ is not known *a priori* from theoretical considerations, then these three spectral densities appear very similar. Thus, some of the

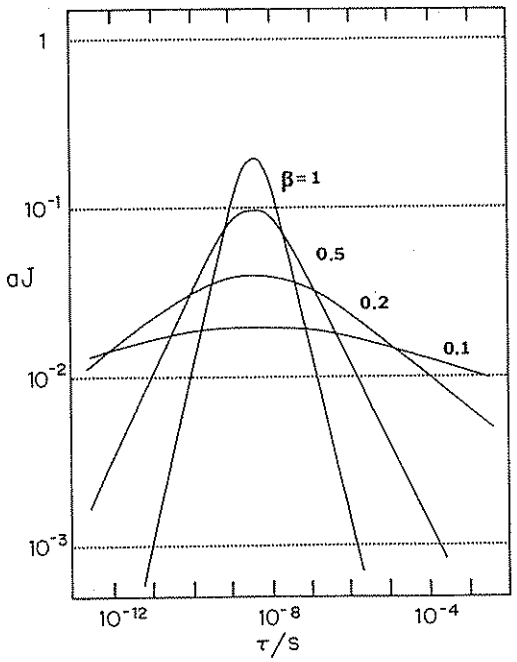

Fig. 15. Log–log plot of $aJ_{\mathrm{FK}}(\omega, \tau, \beta)$ vs. characteristic correlation time τ at the Larmor frequency $\omega/(2\pi) = 40$ MHz and for several width parameters β as shown. The spectral density J_{FK} results from a Fuoss–Kirkwood distribution of correlation times. The middle two values of β used here are the same as those used to generate the two distributions in fig. 13. The normalization $a = \omega_1^{-1} = [(2\pi)\ 8\ \mathrm{MHz}]^{-1}$ such that $J_{\mathrm{BPP,\,max}} = 1$ at 8 MHz.

many single frequency NSR data presented in the literature and fitted with a BPP spectral density may be better fitted by a FK or CC spectral density. Comparisons between $\theta_{FK}(z, \beta)$ (fig. 13) and $\theta_{CC}(z, \delta)$ (fig. 5) show that for a given $\delta = \beta$, the distribution of correlation times is broader for CC than for FK. Such comparisons help to determine the relationship between δ (CC) and β (FK) for the different spectral densities. For both $\omega\tau \ll 1$ and $\omega\tau \gg 1$, the ratio $J_{FK}/J_{CC} \rightarrow 1$ as β and $\delta \rightarrow 1$ and $\rightarrow 2/\pi$ as β and $\delta \rightarrow 0$. For a given substance, or at least a given sample with a specific thermal history [146, 147], δ or β will usually be constant in which case it is not possible to distinguish between J_{FK} and J_{CC} in a NSR Zeeman study unless the frequency dependence is observed.

6.8. *Bryn Mawr (BM)*

The DC spectral density (section 6.5) fits R vs. T data in many molecular solids. It often fits both the τ (or, experimentally, the temperature) and the ω-dependence of the $\omega\tau \ll 1$ (high T) and $\omega\tau \gg 1$ (low T) regions of the observed relaxation rate very well. However, it sometimes fails in the vicinity of R_{max} and the BM spectral density was invented to rectify this. In terms of the short and long correlation time limits, the following restrictive properties seem quite general in a wide variety of molecular solids: (a) J is independent of ω for $\omega\tau \ll 1$; (b) $J \propto \omega^{1-\varepsilon}$ with $0 < \varepsilon \leq 1$ for $\omega\tau \gg 1$; (c) the ratio of the magnitudes of the $\omega\tau \gg 1$ to $\omega\tau \ll 1$ slopes for $\ln J$ vs. $\ln \tau$ is $\varepsilon \leq 1$, the same ε as in condition (b). The DC spectral density satisfies these criteria. For the DC spectral density, fitting the experimental data at any frequency with the high and low temperature data ($\omega\tau \ll 1$ and $\omega\tau \gg 1$, respectively) completely determines all the parameters (i.e., ε, or, also using eq. (45), ε, τ_∞ and E) and R vs. T^{-1} (or J vs. τ) near $\omega\tau \sim 1$ can be predicted with no adjustable parameters. Also, R vs. T^{-1} at any other ω is completely determined. Alternatively, the frequency and temperature dependence over a small temperature range in the $\omega\tau \gg 1$ regime also completely determines all the parameters. This could be important if the sample melts before the $\omega\tau \ll 1$ regime is reached. In any event, measuring R in all τ regions at several frequencies tends to over-determine the J resulting from simple models and since J_{DC} is so successful for $\omega\tau \ll 1$ and $\omega\tau \gg 1$, it suggests that the distribution $\theta_{DC}(z)$ in eq. (55) is close to a more universal distribution of correlation times, or, equivalently, close to the Fourier transform of a correlation function $G(t)$ that is, in some fundamental sense, even more universal for dynamical processes in solids than is the exponential correlation function that results from the assumption of Poisson statistics. The HN (or DH) spectral density discussed in section 6.3 is not a candidate because it does not, in general, satisfy condition (a) discussed above. This is clear from fig. 2.

The BM spectral density originates from a theoretical exercise designed to find the most general J which satisfies the $\omega\tau \ll 1$ and $\omega\tau \gg 1$ properties discussed above [148]. There are many forms for J which satisfy the three criteria stated above. The simplest forms will contain one more parameter than J_{DC} and this parameter η will primarily effect J in the vicinity of $\omega\tau \sim 1$. We investigate one of the simplest of this set of spectral densities [148];

$$J_{BM}(\omega, \tau, \varepsilon, \eta) = f(\varepsilon, \eta)\, \frac{2\tau}{1 + \omega^2\tau^2}\, (1 + \omega^\eta \tau^\eta)^{(1-\varepsilon)/\eta}\,; \tag{71}$$

with $0 < \varepsilon \leq 1$, and $0 < \eta < \infty$. The distribution $\Lambda_{BM}(\xi, \tau, \varepsilon, \eta)$ can, in principle, be obtained numerically from eqs. (35) and (71) by doing an inverse Fourier transform and the procedure for doing so is outlined by Fuoss and Kirkwood [144].

The normalization $f(\varepsilon, \eta)$ must be determined by integrating eq. (71) numerically using eq. (25). It is convenient to define

$$f^*(\varepsilon, \eta) = f(\varepsilon, \eta)/f(\varepsilon, \infty) \tag{72}$$

because $f(\varepsilon, \infty)$ can be determined in closed form;

$$f(\varepsilon, \infty) = [\tfrac{1}{2} + I(\varepsilon)]^{1/2}, \tag{73}$$

with

$$I(\varepsilon) = \frac{1}{\sin(\varepsilon\pi/2)} + \frac{1}{\pi}\sum_{k=1}^{\infty}(-1)^k\left[\frac{1}{k-\varepsilon/2}\right]. \tag{74}$$

The function $f(\varepsilon, \infty)$ varies smoothly from $f(1, \infty) = 1$ to $f(0, \infty) = 0$. The sum in eq. (74) converges slowly and 10,000 terms give an accuracy of 0.01%.

For $\omega\tau \ll 1$ and $\omega\tau \gg 1$,

$$J_{\mathrm{BM}}(\omega, \tau, \varepsilon, \eta) = f(\varepsilon, \eta)2\tau\,, \quad \omega\tau \ll 1\,; \tag{75}$$

and

$$J_{\mathrm{BM}}(\omega, \tau, \varepsilon, \eta) = f(\varepsilon, \eta)2\tau^{-\varepsilon}\omega^{-(1+\varepsilon)}\,. \tag{76}$$

In fig. 16, $\ln J_{\mathrm{BM}}$ vs. $\ln \tau$ is shown for the three frequencies for $\varepsilon = 0.1$ and $\eta = 0.2$. This shows that when both ε and η are small the linear $\omega\tau \gg 1$ regime (eq. 76) is not reached until τ becomes very large (i.e., off-scale on fig. 16). For fixed small ε, this high τ curvature vanishes above $\eta \sim 0.5$ as shown in fig. 17 which shows $\ln J_{\mathrm{BM}}$ vs. $\ln \tau$ for $\varepsilon = 0.1$ and for several values of ε. Values of η above ~ 10 are indistinguishable from $\eta = \infty$. Likewise, for fixed small η, the high τ curvature vanishes above $\varepsilon \sim 0.5$ as shown in fig. 18 which shows $\ln J_{\mathrm{BM}}$ vs. $\ln \tau$ for $\eta = 0.2$ and for several values of ε. For ε and η simultaneously larger, the curvature disappears altogether. Finally, the case $\eta \to \infty$ (i.e., $\eta > 10$) is very similar to the DC case, even for small ε, and the two would be indistinguishable in an experiment. This is shown in fig. 19 which compares J_{BM} $(\eta \to \infty)$ and J_{DC} both with $\varepsilon = 0.2$. (For mathematical completeness, we note that J_{BM} for $\eta \to \infty$ is continuous at $\omega\tau = 1$ but it is not differentiable.) As can be seen from figs. 17 and 18, the value of τ for which J_{BM} is a maximum does not vary from ω^{-1} very much.

6.9. Wagner or log–Gaussian (WAG)

It is natural to investigate a Gaussian distribution of activation energies [85]. The Wagner distribution [149] of correlation parameters $\theta_{\mathrm{WAG}}(z, \alpha)$ is given by

$$\theta_{\mathrm{WAG}}(z, \alpha) = (\alpha/\pi^{1/2})\exp(-\alpha^2 z^2)\,; \tag{77}$$

with $0 < \alpha < \infty$. This leads to a log–Gaussian distribution $\Lambda_{\mathrm{WAG}}(\xi, \tau, \alpha)$ of correlation times ξ since

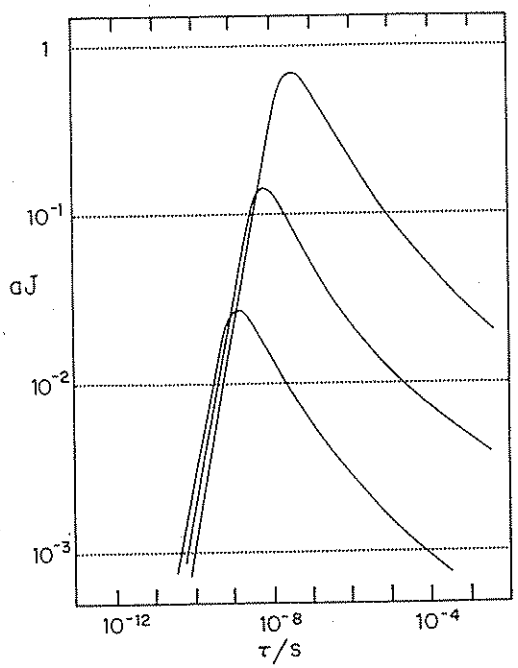

Fig. 16. Log–log plot of $aJ_{BM}(\omega, \tau, \varepsilon, \eta)$ vs. characteristic correlation time τ for width parameters $\varepsilon = 0.1$ and $\eta = 0.2$ at Larmor frequencies of $\omega/(2\pi) = 8$ (top), 40 (middle) and 200 MHz (bottom). The normalization $a = \omega_1^{-1} = [(2\pi)\ 8\ \text{MHz}]^{-1}$ such that $J_{BPP,\,max} = 1$ at 8 MHz.

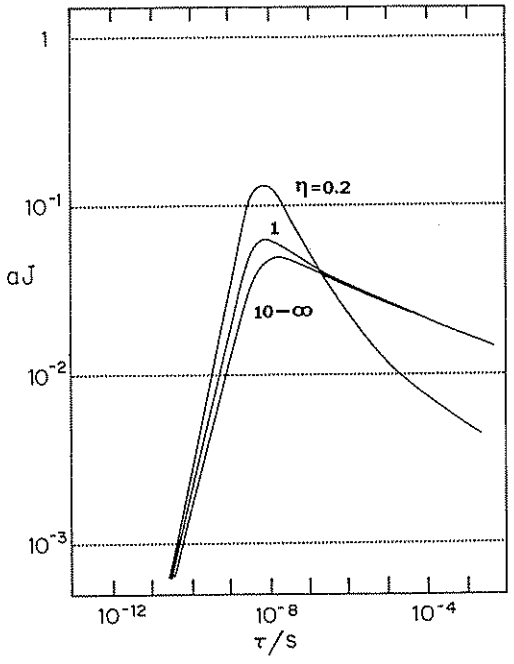

Fig. 17. Log–log plot of $aJ_{BM}(\omega, \tau, \varepsilon, \eta)$ vs. characteristic correlation time τ at the Larmor frequency $\omega/(2\pi) = 40$ MHz and $\varepsilon = 0.1$ for several values of η as shown. The normalization $a = \omega_1^{-1} = [(2\pi)\ 8\ \text{MHz}]^{-1}$ such that $J_{BPP,\,max} = 1$ at 8 MHz.

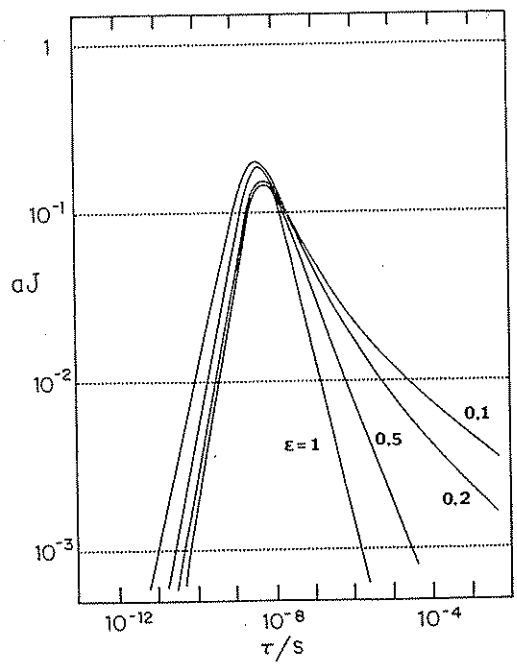

Fig. 18. Log–log plot of $aJ_{BM}(\omega, \tau, \varepsilon, \eta)$ vs. characteristic correlation time τ at the Larmor frequency $\omega/(2\pi) = 40$ MHz and $\eta = 0.2$ for several values of ε as shown. The normalization $a = \omega_1^{-1} = [(2\pi)\ 8\ \text{MHz}]^{-1}$ such that $J_{BPP,\,max} = 1$ at 8 MHz.

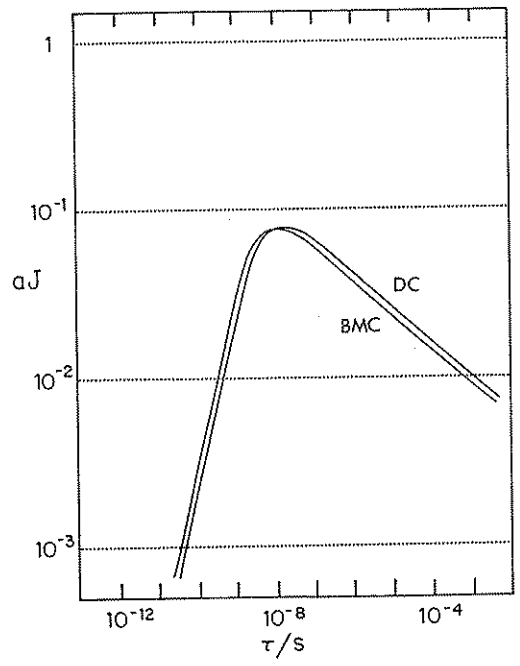

Fig. 19. Log–log plot comparing $aJ_{DC}(\omega, \tau, \varepsilon)$ vs. upper cutoff correlation time τ with $aJ_{BM}(\omega, \tau, \varepsilon, \eta)$ vs. characteristic correlation time τ at the Larmor frequency $\omega/(2\pi) = 40$ MHz with width parameters $\varepsilon = 0.2$ (both DC and BM) and $\eta \to \infty$ (BM). The normalization $a = \omega_1^{-1} = [(2\pi)\ 8\ \text{MHz}]^{-1}$ such that $J_{BPP,\,max} = 1$ at 8 MHz.

$z = \ln(\xi/\tau)$. The parameter τ is a characteristic correlation time and the parameter α is a width parameter.

If eq. (39) is used for ξ and eq. (45) is used for τ with fixed $\xi_\infty \equiv \tau_\infty$, a Gaussian distribution of activation energies ζ results. In this case, the correlation parameter z is also given by $z = [E(\xi) - E(\tau)]/kT$ and is a reduced, inverse temperature, normalized by a difference activation temperature $[E(\xi) - E(\tau)]/k$. Although these assumptions are inherent in the phenomenological development of θ_{WAG} and this is the origin of the distribution θ_{WAG} [149], we emphasize that they need not be made here. The characteristic correlation time τ is the independent variable in the spectral density for this study.

The symmetric distribution $\theta_{WAG}(z)$ of correlation parameters z is shown in fig. 20 for $\alpha = 0.4$ (the narrower of the two) and $\alpha = 0.1$. These values are chosen to have θ_{WAG} approximate θ_{CC} in fig. 5 and θ_{FK} in fig. 13. The spectral density $J_{WAG}(\omega, \tau, \alpha)$ is expressed as an integral using eqs. (35), (40) and (77) and is

$$J_{WAG}(\omega, \tau, \alpha) = \int_{-\infty}^{\infty} \left[\frac{\alpha}{\pi^{1/2}} e^{-\alpha^2 z^2}\right]\left[\frac{2\tau e^z}{1 + \omega^2\tau^2 e^{2z}}\right] dz. \tag{78}$$

This spectral density has been used in a variety of NSR studies in liquids [150, 151] and solids [152, 153]. Equation (78) must be integrated numerically and although tables are available [154, 155] it is faster to use a microcomputer. Ln J_{WAG} vs. ln τ for the three frequencies is shown in fig. 21 for $\alpha = 0.4$ and ln J_{WAG} vs. ln τ for three values of α is shown in fig. 22. As $\alpha \to \infty$ ($\gtrsim 10$), $J_{WAG} \to J_{BPP}$ as expected.

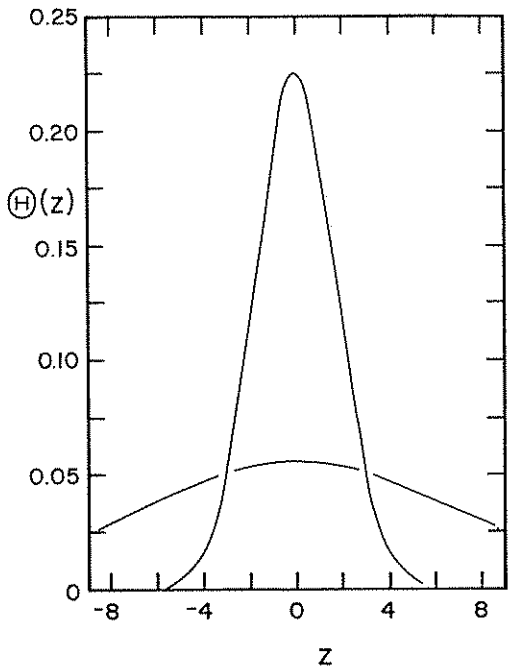

Fig. 20. $\theta_{WAG}(z, \alpha)$ vs. z for $\alpha = 0.4$ (top) and 0.1 (bottom). The Wagner or log–Gaussian distribution $A_{WAG}(\xi, \tau, \alpha)$ of correlation times ξ is characterized by $\theta_{WAG}(z, \alpha)$ with $z = \ln(\xi/\tau)$ for characteristic correlation time τ and width parameter α.

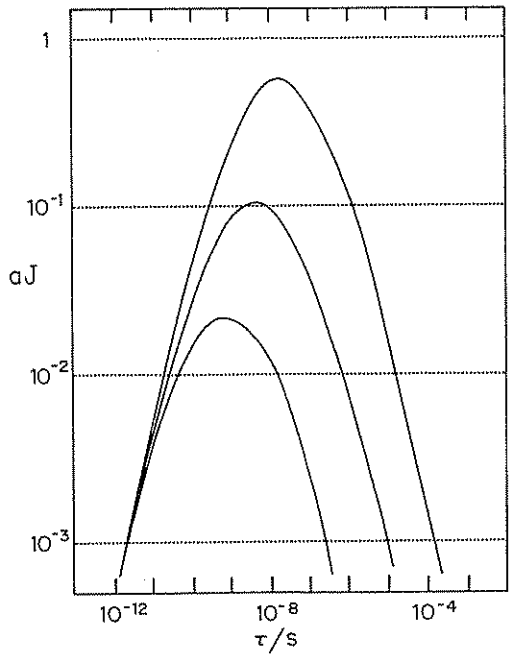

Fig. 21. Log–log plot of $aJ_{WAG}(\omega, \tau, \alpha)$ vs. characteristic correlation time τ for width parameter $\alpha = 0.4$ at Larmor frequencies of $\omega/(2\pi) = 8$ (top), 40 (middle) and 200 MHz (bottom). The spectral density J_{WAG} results from a Gaussian distribution of activation energies or a log–Gaussian distribution of correlation times. The value of α used here is the same as that used to generate the top curve in fig. 20. The normalization $a = \omega_1^{-1} = [(2\pi)\ 8\ \text{MHz}]^{-1}$ such that $J_{BPP,\,max} = 1$ at 8 MHz.

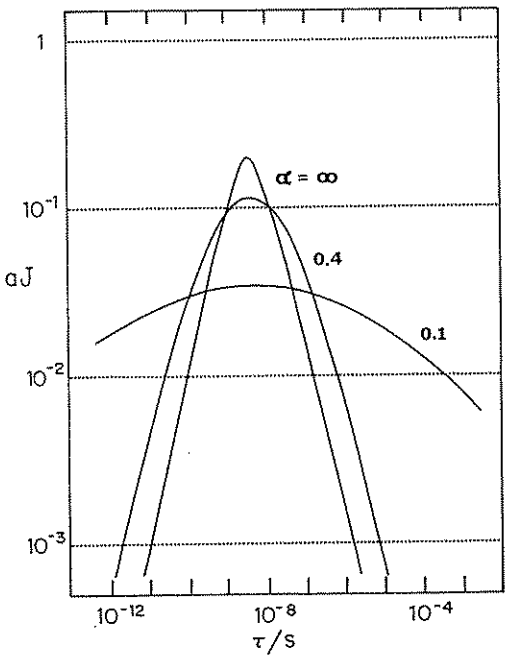

Fig. 22. Log–log plot of $aJ_{WAG}(\omega, \tau, \alpha)$ vs. characteristic correlation time τ at the Larmor frequency $\omega/(2\pi) = 40$ MHz for width parameters α as shown. The spectral density J_{WAG} results from a Gaussian distribution of activation energies or a log–Gaussian distribution of correlation times. The values $\alpha = 0.4$ and 0.1 are the same as those used to generate the two distributions in fig. 20. The normalization $a = \omega_1^{-1} = [(2\pi)\ 8\ \text{MHz}]^{-1}$ such that $J_{BPP,\,max} = 1$ at 8 MHz.

Ln J_{WAG} vs. ln τ is always symmetric about $\omega\tau = 1$ and the limiting values are

$$J_{WAG}(\omega, \tau, \alpha) = \left[\exp\left(\frac{1}{4\alpha^2}\right)\right] 2\tau\,, \quad \omega\tau \ll 1\,; \tag{79}$$

and

$$J_{WAG}(\omega, \tau, \alpha) = \left[\exp\left(\frac{1}{4\alpha^2}\right)\right] 2\tau^{-1}\omega^{-2}\,, \quad \omega\tau \gg 1\,. \tag{80}$$

The $\omega\tau \ll 1$ frequency independent limit is only just reached in fig. 21 and the $\omega\tau \gg 1$ limit is only really evident for the lowest frequency plot (highest curve) in fig. 21. Ln J_{WAG} vs. ln τ is wider in the wings and lower at the maximum than is ln J_{BPP} vs. ln τ but J_{max} occurs at the same $\tau = \omega^{-1}$.

6.10. Log–Lorentzian (LL)

The procedure here is the same as for the Wagner spectral density instead a Lorentzian distribution of correlation parameters is assumed. $\theta_{LL}(z)$ is given by

$$\theta_{LL}(z, \alpha) = \frac{\alpha}{\pi}\,\frac{1}{1 + \alpha^2 z^2}\,; \tag{81}$$

with $0 < \alpha < \infty$, and $\Lambda_{LL}(\xi, \tau, \alpha)$ is a Lorentzian in $\ln(\xi/\tau)$ as the name implies. The parameter τ is a characteristic correlation time and the parameter α is a width parameter. Figure 23 shows $\theta_{LL}(z)$ for $\alpha = 0.71$ (the narrower of the two) and 0.16. These values were chosen to approximately replicate the maximum values of $\theta_{WAG}(z)$ in fig. 20. The spectral density is expressed as an integral using eqs. (35), (40) and (81),

$$J_{LL}(\omega, \tau, \alpha) = \int_{-\infty}^{\infty} \frac{\alpha}{\pi} \left[\frac{1}{1+\alpha^2 z^2}\right]\left[\frac{2\tau\, e^z}{1+\omega^2\tau^2\, e^{2z}}\right] dz\,. \tag{82}$$

Ln J_{LL} vs. ln τ for the three frequencies is shown in fig. 24 for $\alpha = 0.71$. At $\omega\tau \ll 1$ and $\gg 1$ the curvature is of the opposite sign than for J_{WAG} (fig. 21) but like J_{WAG}, J_{LL} is symmetric (in ln τ) about $J_{LL,\,max}$. Ln J_{LL} vs. ln τ for several values of α is shown in fig. 25. As $\alpha \to \infty$ ($\gtrsim 10^4$), $J_{LL} \to J_{BPP}$ as expected. As suggested by fig. 24, J_{LL} does not approach $J \propto \tau^p$ for $\omega\tau \ll 1$ or $J \propto \tau^{-q}$ for $\omega\tau \gg 1$ (for some positive constants p and q) like most other spectral densities. This is a familiar property of a Lorentzian function. Like J_{WAG} and J_{BPP}, $J_{LL,\,max} \propto \omega^{-1}$ when $\omega\tau = 1$.

We note that J_{LL} mimics the sum of a BPP spectral density plus a constant spectral density which we only mention because the latter sometimes occurs experimentally when oxygen is present in the solid. Oxygen gives rise to a relaxation rate which is complicated but approximately independent of temperature (i.e., of τ). This usually only occurs if the material is a liquid at room (or at the stored) temperature. One can distinguish between the two cases by removing any dissolved oxygen.

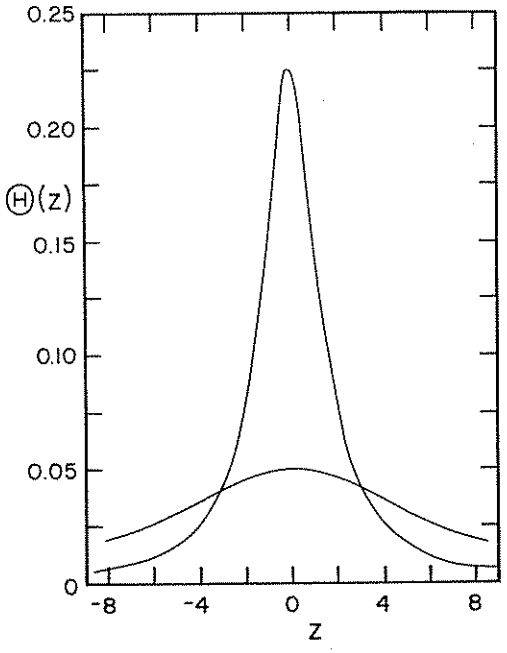

Fig. 23. $\theta_{LL}(z, \alpha)$ vs. z for $\alpha = 0.71$ (top) and 0.16 (bottom). The log–Lorentzian distribution $\Lambda_{LL}(\xi, \tau, \alpha)$ of correlation times ξ is characterized by $\theta_{LL}(z, \alpha)$ with $z = \ln(\xi/\tau)$ for characteristic correlation time τ and width parameter α.

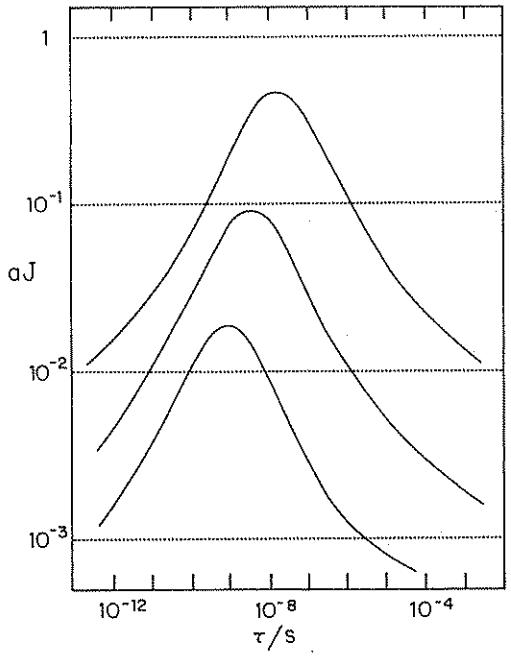

Fig. 24. Log–log plot of $aJ_{LL}(\omega, \tau, \alpha)$ vs. characteristic correlation time τ for width parameter $\alpha = 0.71$ at Larmor frequencies of $\omega/(2\pi) = 8$ (top), 40 (middle) and 200 MHz (bottom). The spectral density J_{LL} results from a Lorentzian distribution of activation energies or a log–Lorentzian distribution of correlation times. The value of α used here is the same as that used to generate the top curve in fig. 23. The normalization $a = \omega_1^{-1} = [(2\pi)\ 8\,\text{MHz}]^{-1}$ such that $J_{BPP,\,max} = 1$ at 8 MHz.

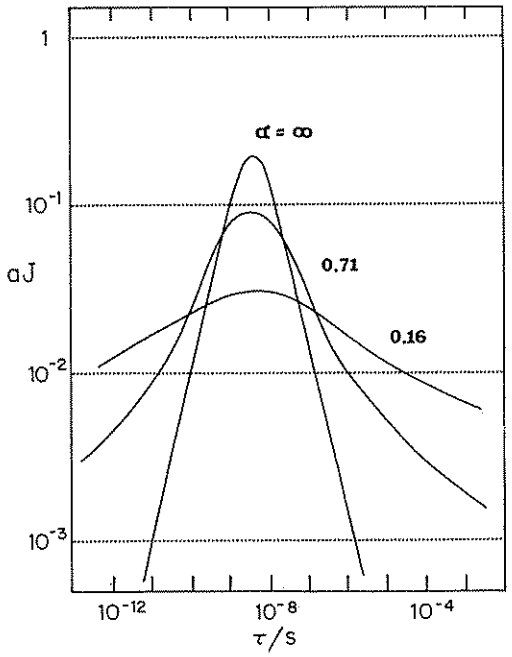

Fig. 25. Log–log plot of $aJ_{LL}(\omega, \tau, \alpha)$ vs. characteristic correlation time τ at the Larmor frequency $\omega/(2\pi) = 40$ MHz for width parameters α as shown. The spectral density J_{LL} results from a Lorentzian distribution of activation energies or a log–Lorentzian distribution of correlation times. The values $\alpha = 0.71$ and 0.16 are the same as those used to generate the two distributions in fig. 23. The normalization $a = \omega_1^{-1} = [(2\pi)\ 8\ \text{MHz}]^{-1}$ such that $J_{BPP,max} = 1$ at 8 MHz.

6.11. *Fröhlich or energy box (FRO)*

The Fröhlich spectral density [84] has been used to interpret NSR data in solids [156, 157]. It is very useful because it is convenient to handle mathematically and any arbitrary spectral density can be conveniently expressed as a sum of Fröhlich spectral densities [156]. Thus, it can be used to investigate the characteristics of all other spectral densities.

The most convenient starting point is to define a distribution $\Gamma(\zeta)$ of activation energies ζ by

$$\begin{aligned} \Gamma_{FRO}(\zeta, E, \Delta) &= 1/(2\Delta)\,, \quad E - \Delta < \zeta < E + \Delta\,; \\ &= 0\,, \qquad \text{otherwise}\,; \end{aligned} \tag{83}$$

with $\Delta < E$. Thus, Γ_{FRO} is a box of height $(2\Delta)^{-1}$ and width 2Δ centered around $\zeta = E$. It has unit area. This distribution of activation energies ζ is related to the distribution of correlation times ξ or correlation parameters z by

$$\Gamma_{FRO}(\zeta)\,\mathrm{d}\zeta = \Lambda_{FRO}(\xi)\,\mathrm{d}\xi = \theta_{FRO}(z)\,\mathrm{d}z \tag{84}$$

and one can compute Λ_{FRO} and θ_{FRO} from Γ_{FRO} and vice versa if $\xi(\zeta)$ is known. If an Arrhenius equation $\xi = \tau_\infty \exp(\zeta/kT)$, where $\xi_\infty = \tau_\infty$ is taken to be constant, is assumed then $\theta_{FRO}(z)$ is also a box. *We make this assumption.* The correlation time corresponding to the center of the energy box (i.e., $\zeta = E$) is $\xi = \tau$ with τ given by $\tau = \tau_\infty \exp(E/kT)$ (eq. (45)). The parameter τ becomes a characteristic correlation time. The distribution functions $\theta_{FRO}(z)$ and $\Lambda_{FRO}(\xi)$ are straightforward to obtain but care

must be taken in relating the parameters which characterize their cutoff values. The distribution $\theta_{\mathrm{FRO}}(z)$ is given by

$$\theta_{\mathrm{FRO}}(z, Z) = 1/(2Z)\,, \quad -Z < z < Z\,;$$
$$= 0\,, \qquad \text{otherwise}\,; \tag{85}$$

where

$$Z = (\Delta/E)\ln(\tau/\tau_\infty)\,, \quad \tau_\infty < \tau\,;$$

or, equivalently,

$$Z = \Delta/(kT)\,, \quad \Delta < E\,;$$

where eqs. (39) and (45) are used with $\xi_\infty \equiv \tau_\infty$. The distribution Λ_{FRO} is given by

$$\Lambda_{\mathrm{FRO}}(\xi, Z, \tau) = [1/(2Z)](1/\xi)\,, \quad \tau\,\mathrm{e}^{-Z} < \xi < \tau\,\mathrm{e}^{Z}\,;$$
$$= 0\,, \qquad \text{otherwise}\,. \tag{86}$$

The upper and lower cutoffs for Λ_{FRO} can be written in other useful ways as discussed below. The function $\theta_{\mathrm{FRO}}(z, Z)$ is shown in fig. 26 for $Z = 3.0$ (narrowest), 5.3 and 7.6. These values are chosen to give $\theta_{\mathrm{FRO}}(z)$ widths comparable with the other distributions investigated.

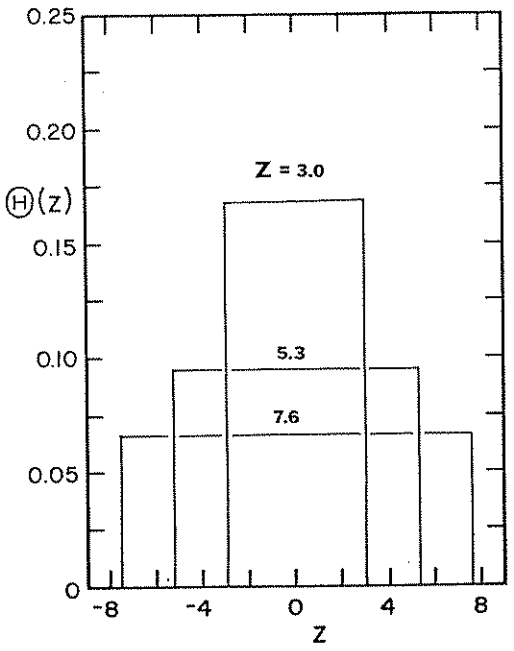

Fig. 26. $\theta_{\mathrm{FRO}}(z, Z)$ vs. z for three values of Z as shown. The Fröhlich distribution $\Lambda_{\mathrm{FRO}}(\xi, \tau, Z)$ of correlation times ξ is characterized by $\theta_{\mathrm{FRO}}(z, Z)$ with $z = \ln(\xi/\tau)$ for characteristic correlation time τ and width parameter Z.

Two independent constants in addition to ω and τ are needed to specify J_{FRO}. It is convenient to choose them to be $\varepsilon = \Delta/E < 1$ and τ_∞ where τ_∞ is the infinite temperature correlation time (or the pre-exponential factor) in eq. (45). Thus τ_∞ is common to all correlation times in the distribution since $\xi_\infty \equiv \tau_\infty$. J_{FRO} becomes

$$J_{\mathrm{FRO}}(\omega, \tau, \tau_\infty, \varepsilon) = \frac{1}{\varepsilon\omega \ln(\tau/\tau_\infty)} \left\{ \arctan\left[\omega\tau \left(\frac{\tau}{\tau_\infty} \right)^{\varepsilon} \right] - \arctan\left[\omega\tau \left(\frac{\tau}{\tau_\infty} \right)^{-\varepsilon} \right] \right\} \tag{87}$$

If we were studying the properties of the Fröhlich spectral density independently of the others being reported here, the three parameters ω, τ/τ_∞ and ε would suffice. However, we want to keep τ separate as the independent variable for the spectral density in order to compare J_{FRO} with the other spectral densities presented in this paper.

Ln J_{FRO} vs. ln τ for the three frequencies is shown in fig. 27 for $\varepsilon = 0.5$ and $\tau_\infty = 10^{-13}$ s. The value $\tau_\infty = 10^{-13}$ s is typical for many dynamical processes involving ^{1}H in solids. The parameter $\omega\tau_\infty = 2.51 \times 10^{-5}$ (where $\omega = 2\pi$ (40 MHz) is our "standard" angular Larmor frequency) is perhaps more relevant than just τ_∞. With these choices for ε and τ_∞, the three distributions $\theta_{\mathrm{FRO}}(z, Z)$ in fig. 26 correspond to the τ values 4×10^{-11} s ($Z = 3.0$), 4×10^{-9} s ($Z = 5.3$) and 4×10^{-7} s ($Z = 7.6$) in fig. 27. Ln J_{FRO} vs. ln τ at $\omega = 2\pi$ (40 MHz) and for several values of ε is shown in fig. 28. As $\varepsilon \to 0$ ($\Delta \to 0$), $J_{\mathrm{FRO}} \to J_{\mathrm{BPP}}$ and as $\varepsilon \to 1$ ($\Delta \to E$), J_{FRO} tends to mimic J_{BMC} for small ε and η.

Investigating the limiting regimes of J_{FRO} is somewhat less straightforward than most of the other spectral densities because $\omega\tau$ must be compared with $\omega\tau_\infty$ as well as with unity. For this and other

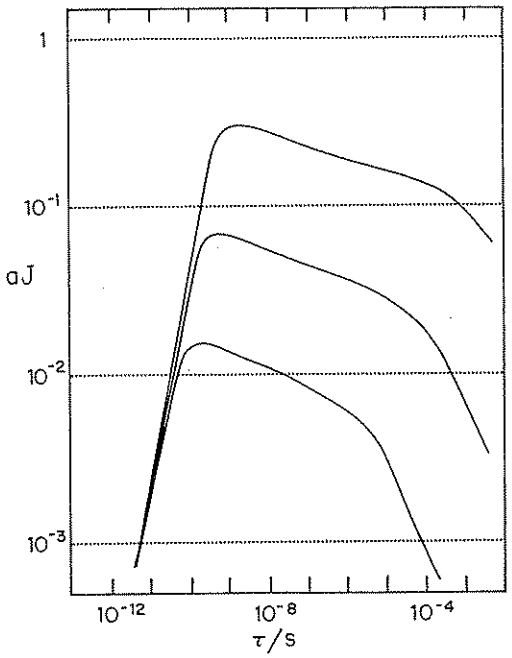

Fig. 27. Log–log plot of $aJ_{\mathrm{FRO}}(\omega, \tau, \tau_\infty, \varepsilon)$ vs. characteristic correlation time τ for width parameter $\varepsilon = 0.5$ and infinite temperature correlation time $\tau_\infty = 10^{-13}$ s at Larmor frequencies of $\omega/(2\pi) = 8$ (top), 40 (middle) and 200 MHz (bottom). The spectral density J_{FRO} results from a Fröhlich or energy box distribution of activation energies ξ. The width of the box is 2Δ and the center of the box is E. The parameter ε is defined by $\varepsilon = \Delta/E$. The three distributions in fig. 26 correspond to the τ values 4×10^{-11} s ($Z = 3.0$), 4×10^{-9} s ($Z = 5.3$) and 4×10^{-7} s ($Z = 7.6$) in this figure. The width of the box in z in fig. 26 depends on τ and τ_∞ in addition to ε. The normalization $a = \omega_1^{-1} = [(2\pi)\ 8\ \mathrm{MHz}]^{-1}$ such that $J_{\mathrm{BPP,\,max}} = 1$ at 8 MHz.

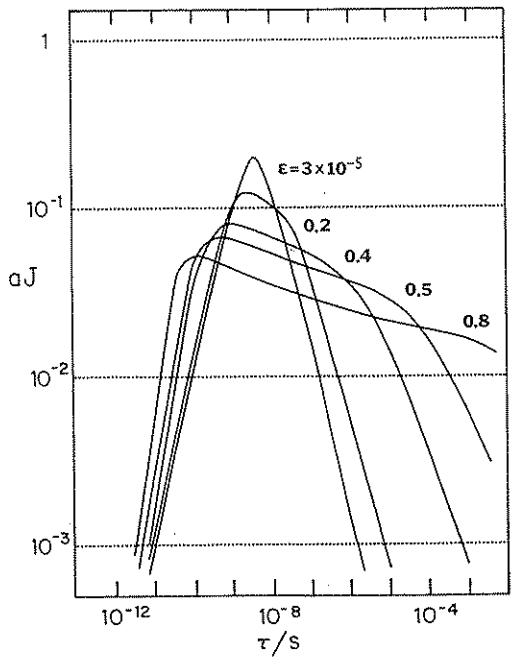

Fig. 28. Log–log plot of $aJ_{\mathrm{FRO}}(\omega, \tau, \tau_\infty, \varepsilon)$ vs. characteristic correlation time τ at the frequency $\omega/(2\pi) = 40$ MHz for infinite temperature correlation time $\tau_\infty = 10^{-13}$ s and for several values of ε as shown. The spectral density J_{FRO} results from a Fröhlich or energy box distribution of activation energies ζ. The parameter ε is defined by $\varepsilon = \Delta/E$. The width of the box is 2Δ and the center of the box is E. The normalization $a = \omega_1^{-1} = [(2\pi)\ 8\,\mathrm{MHz}]^{-1}$ such that $J_{\mathrm{BPP,\,max}} = 1$ at 8 MHz.

practical reasons related to the analysis of experiments, it is convenient to define the limits τ_1 and τ_2 for $\Lambda_{\mathrm{FRO}}(\xi, Z, \tau)$ in eq. (86) by

$$\tau_1 = \tau(\tau/\tau_\infty)^{-\varepsilon} = \tau_\infty\, \mathrm{e}^{(E-\Delta)/kT} = \tau\, \mathrm{e}^{-Z} \tag{88}$$

and

$$\tau_2 = \tau(\tau/\tau_\infty)^{\varepsilon} = \tau_\infty\, \mathrm{e}^{(E+\Delta)/kT} = \tau\, \mathrm{e}^{Z}\,, \tag{89}$$

in which case,

$$\begin{aligned} \Lambda_{\mathrm{FRO}}(\xi, \tau_1, \tau_2) &= \frac{1}{\ln(\tau_2/\tau_1)}\,\frac{1}{\xi}\,, \quad \tau_1 < \xi < \tau_2\,, \\ &= 0\,, \qquad\qquad \text{otherwise}\,, \end{aligned} \tag{90}$$

and the spectral density in eq. (87) takes on the form

$$J_{\mathrm{FRO}}(\omega, \tau_1, \tau_2) = \frac{2}{\omega\,\ln(\tau_2/\tau_1)}\,[\arctan(\omega\tau_2) - \arctan(\omega\tau_1)] \tag{91}$$

The plotting parameter τ (the same as previously used) is just the geometric mean of the cutoff τ values;

$$\tau = (\tau_1 \tau_2)^{1/2} . \tag{92}$$

The condition $\tau_\infty < \tau_1 < \tau < \tau_2$ is always true. In the limit $\omega\tau_1 < \omega\tau_2 \ll 1$,

$$J_{\mathrm{FRO}}(\omega, \tau_1, \tau_2) = \frac{2(\tau_2 - \tau_1)}{\ln(\tau_2/\tau_1)} \tag{93}$$

which is frequency independent and can be seen in fig. 27 at small τ values. Equation (93) reduces to $J_{\mathrm{BPP}} = 2\tau$ in the limit $\tau \equiv \tau_2 \gg \tau_1$. In the limit $1 \ll \omega\tau_1 < \omega\tau_2$,

$$J_{\mathrm{FRO}}(\omega, \tau_1, \tau_2) = \frac{2}{\omega^2 \ln(\tau_2/\tau_1)} \left(\frac{1}{\tau_1} - \frac{1}{\tau_2} \right) . \tag{94}$$

This region is observable for several of the curves characterized by small ε in fig. 28 and it is only just observable at large τ for the largest ω in fig. 27 (bottom curve). If $\tau_2 \to \tau_1 \equiv \tau$ then J_{FRO} in eq. (94) becomes $J_{\mathrm{BPP}} = 2/(\omega^2\tau)$. If τ_1 and τ_2 are sufficiently different and the condition $\omega\tau_1 \ll 1 \ll \omega\tau_2$ is satisfied,

$$J_{\mathrm{FRO}}(\omega, \tau_1, \tau_2) = \frac{\pi}{\omega \ln(\tau_2/\tau_1)} . \tag{95}$$

This is the case in the intermediate regions in fig. 27.

The parameters τ_1 and τ_2 can be labelled with an additional subscript i and any distribution of correlation times can be expressed as

$$\Lambda(\xi, \tau_{11}, \tau_{21}, \ldots, \tau_{1N}, \tau_{2N}) = \sum_{i=1}^{N} a_i \Lambda_{\mathrm{FRO}}(\xi, \tau_{1i}, \tau_{2i}) , \tag{96}$$

with the width $\tau_{2i} - \tau_{1i}$, independent of i, being some monotonically decreasing function of N (in the same way numerical integration is performed) and,

$$\sum_{i=1}^{N} a_i = 1 . \tag{97}$$

A very general spectral density is then

$$J(\omega, \tau_{11}, \tau_{21}, \ldots, \tau_{1N}, \tau_{2N}) = \sum_{i=1}^{N} a_i J_{\mathrm{FRO}}(\omega, \tau_{1i}, \tau_{2i}) . \tag{98}$$

This procedure is very useful for investigating the properties of the various spectral densities and for numerically fitting data. It can be determined *a priori* how many boxes are needed to reproduce the desired spectral density (i.e., the value of N) and no difficult numerical integration need be done. Alternatively, one can fit the data with as few boxes as possible and then see which distribution of correlation times the sum of boxes best mimics. In order for this exercise to be useful, the NSR rates must encompass both long and short correlation time limits and the experiments must be done at several Larmor frequencies.

7. Summary

Following a brief introduction to solid state nuclear spin relaxation (NSR), we have investigated ten spectral densities which are or could be used to interpret NSR rates in solids. We have discussed their mathematical properties in some detail in a manner which allows direct comparisons between them and in a manner which should aid in the interpretation of experiments. Many of the spectral densities investigated have been assumed to arise from a distribution of simple Bloembergen–Purcell–Pound or Debye spectral densities which, in turn, have their origin in random motion of the appropriate molecular or intramolecular geometric parameters. It is the modulation of these vectors and/or angles by the motion which is responsible for NSR. Alternatively, the various spectral densities can be taken as the Fourier transforms of single non-exponential correlation functions which describe non-random motion of the appropriate vectors.

Acknowledgement

Acknowledgement is made to the Donors of the Petroleum Research Fund administered by the American Chemical Society, for the partial support of this research.

References

[1] R.R. Ernst, G. Bodenhausen and A. Wokaun, Principles of Nuclear Magnetic Resonance in One and Two Dimensions (Oxford Univ. Press, Oxford, 1987).
[2] M. Munowitz and A. Pines, Adv. Chem. Phys. 66 (1987) 1.
[3] B.C. Gerstein and C.R. Dybowski, Transient Techniques in NMR of Solids (Academic Press, New York, 1985).
[4] C.H. Wang, Spectroscopy of Condensed Media (Academic Press, New York, 1985).
[5] I. Ando and G.A. Webb, Theory of NMR Parameters (Academic Press, New York, 1983).
[6] C.A. Fyfe, Solid State NMR For Chemists (C.F.C. Press, Guelph, Canada, 1983).
[7] V.J. McBrierty and D.C. Douglass, Phys. Rep. 63 (1980) 61.
[8] D. Wolf, Spin Temperature and Nuclear-Spin Relaxation in Matter (Oxford Univ. Press, Oxford, 1979).
[9] C.P. Slichter, Principles of Nuclear Magnetism (Springer, Berlin, 1978).
[10] H.W. Spiess, NMR: Basic Princ. and Prog. 15 (1978) 55.
[11] M. Mehring, NMR: Basic Princ. and Prog. 11 (1976) 1.
[12] U. Haeberlen, Adv. Magn. Resonance, Supp. 1 (1976) 1.
[13] P.S. Allen, MTP Int. Rev. Sci., Vol. 4, Series I, ed. C.A. McDowell, 1972.
[14] C.P. Poole Jr and H.A. Farach, Relaxation in Magnetic Resonance (Academic Press, New York, 1971).
[15] D.C. Ailion, Adv. Magn. Resonance 5 (1971) 177.
[16] F. Noack, NMR: Basic Princ. and Prog. 3 (1971) 83.
[17] J. Jeener, Adv. Magn. Resonance 3 (1968) 206.
[18] J.M. Deutch and I. Oppenheim, Adv. Magn. Resonance 3 (1968) 43.
[19] R.G. Gordon, Adv. Magn. Resonance 3 (1968) 1.
[20] A.G. Redfield, Adv. Magn. Resonance 1 (1965) 1.
[21] A. Abragam, The Principles of Nuclear Magnetism (Oxford Univ. Press, Oxford, 1961).
[22] E. Meirovitch, S.B. Rananavare and J.H. Freed, J. Phys. Chem. 91 (1987) 5014.
[23] P. Meier, G. Kothe, P. Jonsen, M. Trecoske and A. Pines, J. Chem. Phys. 87 (1987) 6867.
[24] H.W. Spiess, Colloid & Polym. Sci. 261 (1983) 193.
[25] L.P. Ingman, E. Koivula, Z.T. Lalowicz, M. Punkkinen and E.E. Ylinen, J. Chem. Phys. 88 (1988) 58.
[26] R. Janssen, G.A.H. Tijink and W.S. Veeman, J. Chem. Phys. 88 (1988) 518.
[27] J.M. Bernassau, M. Fetizon and J.A. Pinheiro, J. Phys. Chem. 90 (1986) 1051.
[28] H.G. Hertz, Prog. Nucl. Magn. Resonance Spectrosc. 16 (1983) 115.

[29] R.L. Vold and R.R. Vold, Prog. Nucl. Magn. Resonance Spectrosc. 12 (1978) 79.
[30] P.A. Beckmann, J.W. Emsley, G.R. Luckhurst and D.L. Turner, Mol. Phys. 59 (1986) 97.
[31] W. Longueville, M. Bée, J.P. Amoureux and R. Fouret, J. Phys. (France) 47 (1986) 291.
[32] B. Gabrys, F. Horii and R. Kitamaru, Macromol. 20 (1987) 175.
[33] A.D. English, Macromol. 17 (1984) 2182.
[34] D. Suwelack, W.P. Rothwell and J.S. Waugh, J. Chem. Phys. 73 (1980) 2559.
[35] S. Clough, Physica B 136 (1986) 145.
[36] S. Clough, P.J. McDonald and F.O. Zelaya, J. Phys. C 17 (1984) 4413.
[37] P.A. Beckmann, A.M. Cheung, E.E. Fisch, F.A. Fusco, R.E. Herzog and M. Narasimhan, J. Chem. Phys. 84 (1986) 1959.
[38] R.M. Green and A.J. Horsewill, Mol. Phys. 57 (1986) 887.
[39] S. Clough, G.J. Barker, K.J. Abed and A.J. Horsewill, Phys. Rev. Lett. 60 (1988) 136.
[40] D.R. Frankl, Electromagnetic Theory (Prentice-Hall, Englewood Cliffs, New Jersey, 1986).
[41] D.B. Zax, A. Bielecki, K.W. Zilm, A. Pines and D.P. Weitekamp, J. Chem. Phys. 83 (1985) 4877.
[42] G.P. Jones and J.T. Daycock, J. Phys. E 4 (1971) 641.
[43] N.F. Ramsey, Molecular Beams (Oxford Univ. Press, Oxford, 1963).
[44] D.P. Kelley, D.R. Leslie and R.A. Craig, J. Magn. Resonance 52 (1983) 480.
[45] J.R. Reitz, F.J. Milford and R.W. Christy, Foundations of Electromagnetic Theory (Addison-Wesley, London, 1979).
[46] P.A. Beckmann, Mol. Phys. 34 (1977) 665.
[47] M.E. Rose, Elementary Theory of Angular Momentum (Wiley, New York, 1957).
[48] M. Tinkham, Group Theory and Quantum Mechanics (McGraw-Hill, New York, 1964).
[49] G.B. Matson, J. Chem. Phys. 67 (1977) 5152.
[50] E. Fermi, Nuclear Physics (Univ. Chicago Press, Chicago, 1950).
[51] L.I. Schiff, Quantum Mechanics (McGraw-Hill, New York, 1968).
[52] L.K. Runnels, Phys. Rev. A 134 (1964) 28.
[53] R.L. Hilt and P.S. Hubbard, Phys. Rev. A 134 (1964) 392.
[54] J.D. Cutnell and W. Venable, J. Chem. Phys. 60 (1974) 3795.
[55] P.S. Hubbard, J. Chem. Phys. 53 (1970) 985.
[56] E.R. Andrew and D.P. Tunstall, Proc. Phys. Soc. Part I (GB) 78 (1961) 1.
[57] N. Bloembergen, E.M. Purcell and R.V. Pound, Phys. Rev. 73 (1948) 679.
[58] F. Bloch, Phys. Rev. 70 (1946) 460.
[59] R. Kubo and K. Tomita, Proc. Phys. Soc. Jpn. 9 (1954) 888.
[60] K.G. Conn, P.A. Beckmann, C.W. Mallory and F.B. Mallory, J. Chem. Phys. 87 (1987) 20.
[61] P.A. Beckmann, C.I. Ratcliffe and B.A. Dunell, J. Magn. Resonance 32 (1978) 391.
[62] M.D. Dunn and C.A. McDowell, Mol. Phys. 24 (1972) 969.
[63] J. Jeener and P. Broekaert, Phys. Rev. 157 (1967) 232.
[64] C.P. Slichter and D.C. Ailion, Phys. Rev. 135 (1964) A1099.
[65] D.C. Ailion and P.P. Ho, Phys. Rev. 168 (1968) 662.
[66] D.C. Ailion and C.P. Slichter, Phys. Rev. 137 (1965) A235.
[67] K.R. Jeffrey, T.C. Wong, E.E. Burnell, M.J. Thompson, T.P. Higgs and N.R. Chapman, J. Magn. Resonance 36 (1979) 151.
[68] O. Lauer, D. Stehlik and K.H. Hausser, J. Magn. Resonance 6 (1972) 524.
[69] U. Haeberlen, Z. Naturforsch. 25a (1970) 1459.
[70] R. van Steenwinkel, Z. Naturforsch. 24a (1969) 1526.
[71] M.R. Choudhury, J.W. Harrell Jr, J.B. Nielsen and J.S. Thrasher, J. Chem. Phys. 88 (1988) 2135.
[72] T.M. Conner, NMR: Basic Princ. and Prog. 4 (1971) 247.
[73] D.C. Look, I.J. Lowe and J.A. Northby, J. Chem. Phys. 44 (1966) 3441.
[74] D.C. Look and I.J. Lowe, J. Chem. Phys. 44 (1966) 3437.
[75] D.C. Look and I.J. Lowe, J. Chem. Phys. 44 (1966) 2995.
[76] G.P. Jones, Phys. Rev. 148 (1966) 332.
[77] R.E. Wasylishen and K.R. Jeffrey, J. Chem. Phys. 78 (1983) 1000.
[78] D.E. O'Reilly, E.M. Peterson, C.E. Scheie and P.K. Kadaba, J. Chem. Phys. 58 (1973) 3018.
[79] P.A. Beckmann, J.W. Emsley, G.R. Luckhurst and D.L. Turner, Mol. Phys. 50 (1983) 699.
[80] R.L. Vold, W.H. Dickerson and R.R. Vold, J. Magn. Resonance 43 (1981) 213.
[81] Y. Dong, Bull. Magn. Resonance 9 (1987) 29.
[82] A.-H. Beine, E. Dachwitz, L. Wodniok and M. Stockhausen, Z. Naturforsch 41a (1986) 1060.
[83] R.M. Hill and A.K. Jonscher, Contemp. Phys. 24 (1983) 75.
[84] H. Fröhlich, Theory of Dielectrics (Oxford Univ. Press, Oxford, 1958).
[85] K. Kauzmann, Rev. Mod. Phys. 14 (1942) 12.
[86] P. Debye, Polar Molecules (Dover Publ., New York, 1945).

[87] E. Fukushima and S.B.W. Roeder, Experimental Pulse NMR (Addison-Wesley, London, 1981).
[88] J.H. Freed, J. Chem. Phys. 66 (1977) 4183.
[89] H.S. Gutowsky, A. Saika, M. Takeda and D.E. Woessner, J. Chem. Phys. 27 (1957) 534.
[90] L.A. Dissado and R.M. Hill, Philos. Mag. B 41 (1980) 625.
[91] L.A. Dissado and R.M. Hill, Nature 279 (1979) 685.
[92] J.E. Anderson and R. Ullman, 47 (1967) 2178.
[93] S.H. Glarum, J. Chem. Phys. 33 (1960) 639.
[94] L.A. Dissado, Chem. Phys. Lett. 141 (1987) 515.
[95] J.R. Macdonald, Physica 28 (1962) 485.
[96] J.R. Macdonald, J. Chem. Phys. 36 (1962) 345.
[97] E. Rössler and H. Sillescu, Chem. Phys. Lett. 112 (1984) 94.
[98] S. Glasstone, K.J. Laidler and H. Eyring, The Theory of Rate Processes (McGraw-Hill, New York, 1941).
[99] H. Dekker, Phys. Lett. A 113 (1985) 193.
[100] A.K. Rajagopal and F.W. Wiegel, Physica A 127 (1984) 218.
[101] S. Clough, A. Heidemann, A.J. Horsewill, J.D. Lewis and M.N.J. Paley, J. Phys. C 15 (1982) 2495.
[102] R.M. Hill and L.A. Dissado, J. Phys. C 15 (1982) 5171.
[103] O. Edholm and C. Blomberg, Chem. Phys. 56 (1981) 9.
[104] S. Clough and A. Heidemann, J. Phys. C 13 (1980) 3585.
[105] J. Kowalewski and T. Liljefors, Chem. Phys. Lett. 64 (1979) 170.
[106] C. Brot, Chem. Phys. Lett. 3 (1969) 319.
[107] H.A. Resing, Mol. Cryst. Liq. Cryst. 9 (1969) 101.
[108] J.S. Waugh and É.I. Fedin, Sov. Phys. – Solid State 4 (1963) 1633.
[109] S. McGuigan, J.H. Strange and J.M. Chezeau, Mol. Phys. 49 (1983) 275.
[110] S. McGuigan, J.H. Strange and J.M. Chezeau, Mol. Phys. 47 (1982) 373.
[111] T.M. Conner, Trans. Faraday Soc. 60 (1964) 1574.
[112] F. Noack and G. Preissing, Z. Naturforsch. 24a (1969) 143.
[113] V. Graf, F. Noack and M. Stohrer, Z. Naturforsch 32a (1977) 61.
[114] R.M. Hill, J. Mater. Sci. 16 (1981) 118.
[115] R.M. Hill, J. Mater. Sci. 17 (1982) 3630.
[116] K.L. Ngai, A.K. Jonscher, and C.T. White, Nature 277 (1979) 185.
[117] R.M. Hill, Phys. Status Solidi b 103 (1981) 319.
[118] S. Havriliak and S. Negami, J. Polym. Sci. C 14 (1966) 99.
[119] L.A. Dissado, R.R. Nigmatullin and R.M. Hill, Adv. Chem. Phys. 63 (1985) 253.
[120] Y. Shioya and S. Mashimo, J. Chem. Phys. 87 (1987) 3173.
[121] R. Kohlrausch, Ann. Phys. (Germany) 12 (1847) 393.
[122] G. Williams and D.C. Watts, Trans. Faraday Soc. 66 (1970) 80.
[123] J. Budimir and J.L. Skinner, J. Chem. Phys. 82 (1985) 5232.
[124] S. Bozdemir, Phys. Status Solidi b 128 (1985) 119.
[125] E. Helfand, J. Chem. Phys. 78 (1983) 1931.
[126] A.N. Garroway, W.M. Ritchey and W.B. Moniz, Macromol. 15 (1982) 1051.
[127] J.E. Shore and R. Zwanzig, J. Chem. Phys. 63 (1975) 5445.
[128] G. Williams, D.C. Watts, S.B. Dev and A.M. North, Trans. Faraday Soc. 67 (1971) 1323.
[129] K.S. Cole and R.H. Cole, J. Chem. Phys. 9 (1941) 341.
[130] J.-M. Chezeau, J.H. Strange and C. Brot, J. Chem. Phys. 56 (1972) 1380.
[131] D.W. Davidson and R.H. Cole, J. Chem. Phys. 19 (1951) 1484.
[132] P.A. Beckmann, A.M. Cheung, R.E. Herzog, E.E. Fisch, M. Narasimhan, C.W. Mallory and F.B. Mallory, J. Chem. Soc. Faraday Trans. II 81 (1985) 1013.
[133] P.A. Beckmann, F.A. Fusco and A.E. O'Neill, J. Magn. Resonance 59 (1984) 63.
[134] P.A. Beckmann, Chem. Phys. 63 (1981) 359.
[135] W. Müller-Warmuth and W. Otte, J. Chem. Phys. 72 (1980) 1749.
[136] L.J. Burnett and B.H. Muller, J. Magn. Resonance 23 (1976) 343.
[137] S.B.W. Roeder, E.O. Stejskal and W.E. Vaughan 43 (1965) 1317.
[138] P. Fang, Physica 27 (1961) 681.
[139] J.A. Ripmeester, J. Chem. Phys. 85 (1986) 747.
[140] S. Nagaoka, T. Terao, F. Imashiro, A. Saika, N. Hirota and S. Hayashi, J. Chem. Phys. 79 (1983) 4694.
[141] M. Polak and D.C. Ailion, J. Chem. Phys. 67 (1977) 3029.
[142] J.E. Anderson, J. Magn. Resonance 11 (1973) 398.
[143] E. Strick, Adv. Mol. Relax Interaction Processes 24 (1982) 37.

[144] R.M. Fuoss and J.G. Kirkwood, J. Amer. Chem. Soc. 63 (1941) 385.
[145] M. Bée, M. Foulon, J.P. Amoureux, C. Caucheteux and C. Poinsignon, J. Phys. C 20 (1987) 337.
[146] M.C. Aronson, P.A. Beckmann, B.J. Ross and S.L. Tan, Chem. Phys. 63 (1981) 349.
[147] P.S. Allen and C.J. Howard, Mol. Phys. 16 (1969) 311.
[148] A.M. Albano, P.A. Beckmann, M.E. Carrington, F.A. Fusco, A.E. O'Neill and M.E. Scott, J. Phys. C 16 (1983) L979.
[149] K.W. Wagner, Ann. Phys. (Germany) 40 (1913) 817.
[150] P.W. Drake, R. Pridham and R. Meister, J. Chem. Phys. 48 (1968) 2272.
[151] A.G. Favret and R. Meister, J. Chem. Phys. 41 (1964) 1011.
[152] E.R. Andrew, D.J. Bryant, E.M. Cashell and Q.A. Meng, Phys. Lett. A 88 (1982) 487.
[153] E.R. Andrew, D.J. Bryant and E.M. Cashell, Chem. Phys. Lett. 69 (1980) 551.
[154] W.A. Yager, Physics 7 (1936) 434.
[155] A.S. Nowick and B.S. Berry, IBM J. Res. Dev. 5 (1961) 297.
[156] A.M. Albano, P.A. Beckmann, M.E. Carrington, E.E. Fisch, F.A. Fusco, A.E. O'Neill and M.E. Scott, Phys. Rev. B 30 (1984) 2334.
[157] D.W. McCall, D.C. Douglass and E.W. Anderson, J. Chem. Phys. 30 (1959) 1272.